scientific reports

Check for updates

OPEN

Carvacrol from *Moringa oleifera* as a potential antidiabetic agent using integrated in-silico approach inhibiting *TCF7L2*

Amna Saleem[1]✉, Nouman Ali[1,2]✉, Adeeba Ali[1], Erkabay Eshchanov[3] & Shakhlokhon Kurbanova[4]

Diabetes mellitus is a major health concern worldwide; lifestyle and rising urbanization are the key contributing factors. The genetic factors implicated in type 2 diabetes include the transcription factor 7-like 2 (*TCF7L2*) gene on chromosome 10q25.3, which has been greatly linked with diabetes, but the mechanisms and therapeutic effect on this gene are yet to be clearly defined. The objective of the research was to discover and screen natural phytochemicals of *Moringa oleifera*, especially carvacrol, as promising *TCF7L2* inhibitors through combined in-silico methods. We have used a computational pipeline that includes ADMET profiling, molecular docking, molecular, dynamics (MD) simulations, and density functional theory (DFT) analysis. The ADMET analysis demonstrated that carvacrol has desirable pharmacokinetics, such as high gastrointestinal absorption, drug-likeness, and low-predicted oral toxicity. Molecular docking studies showed that carvacrol has a high binding affinity with the TCF7L2 protein with a binding energy of -5.5 kcal/mol. The conformational stability of the carvacrol-TCF7L2 complex was further validated through an extended 200 ns MD simulation, where the protein backbone RMSD stabilized after ~40 ns within ~0.25–0.35 nm (2.5–3.5 A), while the ligand RMSD remained consistently low at ~0.01–0.02 nm (0.1–0.2 A), supported by a persistent hydrogen-bond network throughout the trajectory. The chemical stability and reactivity of the compound were confirmed by DFT calculations. These findings indicate that carvacrol has potential as a lead compound against *TCF7L2* in the treatment of type 2 diabetes. These results are in support of the therapeutic relevance of carvacrol, though experiments are necessary to prove its efficacy and safety in biological systems.

Keywords Diabetes mellitus, TCF7L2, Moringa oleifera, Carvacrol, Molecular dynamics simulations

Diabetes mellitus is a heterogeneous disorder characterized by hyperglycemia resulting from a defect in insulin secretion due to the disturbance of carbohydrates, lipids, and proteins[1]. It has become one of the rising epidemics in the world, estimated to be 366 million in 2011, and 552 million will have the disease by 2030[2]. Diabetes mellitus is a multifactorial disease that is a leading cause of organ damage, dysfunction, and failure involving the kidney, retina, heart, nervous system, and blood vessels[3].

Diabetes is caused by many metabolic factors and the main reason is the destruction of pancreatic beta-cells by autoimmunity. Another reason for diabetes is the resistance of the insulin to the body. Some other abnormalities involve intolerance of glucose production that directly affects pregnant women and other conditions in which particular genetic defects are highly contributing to diabetes mellitus[4]. Despite its significant prevalence, patients are unaware of multifactorial disorders, and the variations in the *TCF7L2* gene are highly responsible for the reduction of beta-cell function, leading to impaired insulin secretion[5]. *TCF7L2* variations disrupt the regulatory functions, which are involved in developing difficulties in maintaining stable blood sugar levels[6].

Variations in the *TCF7L2* gene linked to insulin resistance are considered a major factor in developing type 2 diabetes mellitus[6]. Similarly, the *ABCC8* gene, which helps regulate insulin, has been linked to T2DM[7]. The

[1]Department of Biotechnology, Faculty of Science and Technology, University of Central Punjab, Lahore, Punjab, Pakistan. [2]Department of Molecular Biosciences, Faculty of Physical and Biological Science, Rashid Latif Khan University, Lahore, Punjab, Pakistan. [3]Department of Chemistry, Urgench State University, Urgench, Uzbekistan. [4]Department of Psychology and Medicine, Mamun University, Khiva, Uzbekistan. ✉email: amna.saleem4367@gmail.com; Nouman.ali.anwar336@gmail.com

CAPN10 gene, which codes for enzymes degrading proteins, was the first to show an unequivocal association with T2DM. Its role in insulin secretion, hindered by mutations, is a fascinating aspect of our understanding of the disease[8,9]. These associations illustrate the complexity of T2DM genetic susceptibility, with multiple genes contributing to the overall risk profile of the disease. Notably, while genetic variants engender risk, they do not directly cause disease; our environmental inputs and lifestyle also play a crucial role in influencing disease risk, empowering us to take control of our health. However, most recent studies demonstrated that *TCF7L2* can lead to multiple complications and may contribute to cause diabetes mellitus in early-onset individuals and old age people of the global population. *TCF7L2* gene was located on chromosome 10q25.3 and initially sequenced in cancer cell lines. It is a member of the T-cell factor/lymphoid enhancer binding factor family and is considered the most important potent locus that may lead to developing a risk for Type 2 diabetes mellitus (Fig. 1)[10].

Moringa oleifera essential oil also has carvacrol, a monoterpenoid phenol that has exhibited strong antidiabetic effects in various preclinical models[11,12]. Carvacrol (20 mg/kg/day), given intraperitoneally over 4–6 weeks in streptozotocin (STZ)-induced diabetic mice, produced significant reductions in both random and fasting plasma glucose as well as an improvement in glucose tolerance, along with a decrease in triglyceride levels and the restoration of important hepatic enzymes (hexokinase, phosphofructokinase, and citrate synthase)[13]. Likewise, in STZ-induced type 1 diabetic mice, carvacrol at 10–20 mg/kg/day for up to 6 weeks substantially ameliorated hyperglycemia, and in type 2 diabetic rat models, carvacrol reduced fasting blood glucose and lipid levels and improved gut-derived short-chain fatty acids and GPR41/43 expression[11,14]. In yet another study in STZ-diabetic rats, oral administration of carvacrol at 25 and 50 mg/kg body weight had a modest hypoglycemic effect and a marked beneficial effect on liver enzyme parameters[13]. Mechanistically, carvacrol was found to exert its antidiabetic properties through insulin-sensitizing effects by the PI3K/AKT/GLUT4 signaling, regulation of glucose-metabolizing hepatic enzymes, and by acting on transient receptor potential channels (TRPA1, TRPM7) involved in the secretion of GLP1 and insulin release[12].

TCF7L2 represents the strongest genetic susceptibility locus for type 2 diabetes identified to date; however, unlike classical metabolic enzymes, it remains pharmacologically underexplored. Despite extensive genetic and functional evidence linking TCF7L2 to β-cell dysfunction and impaired insulin secretion, no validated small-molecule modulators have been reported. Targeting TCF7L2 therefore represents a novel upstream strategy aimed at modulating transcriptional regulation of glucose homeostasis rather than inhibiting conventional enzymatic pathways. This study aims to find a potential anti-diabetic drug from the phytochemicals of *Moringa oleifera* that may contribute to treatment, which will provide a useful way to evaluate the cause of disease and

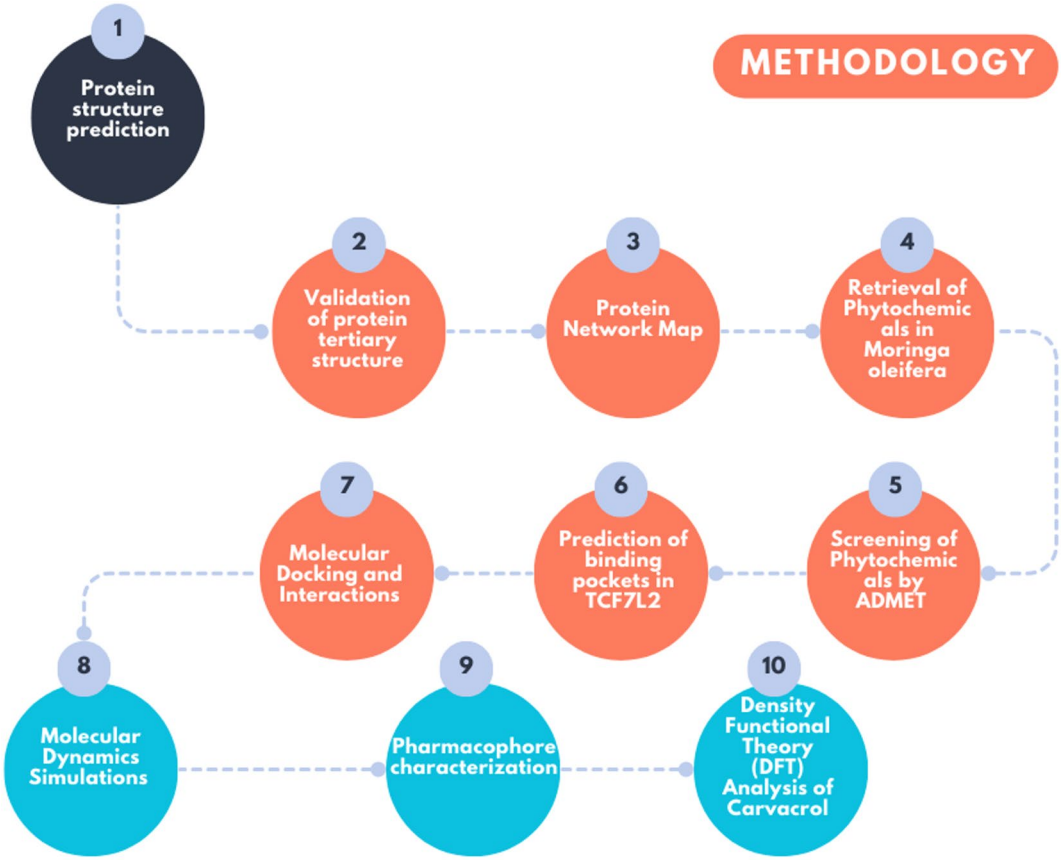

Fig. 1. Workflow of the study. Twenty-five phytochemicals from *Moringa oleifera* were retrieved and screened by ADMET, of which seven were docked against TCF7L2. Carvacrol, the top-ranked ligand, was further validated through MD simulations, identifying it as a potential natural inhibitor of TCF7L2.

identify drug targets using computational approaches. Computational approaches have provided an organized platform for multifactorial defects by developing computer-aided drug design (CADD), a less time-consuming and expensive approach. It will make it easier for medical experts to explore novel lead compounds for further in-vitro and in-vivo trials. Therefore, in-vitro and in-vivo trials are mandatory for the safety and efficacy of drugs designed using computational approaches.

Materials and methods

Protein structure prediction

The selected protein sequence was retrieved from UniProt (https://www.uniprot.org/) protein homology modelling. Robetta (http://robetta.bakerlab.org/) is an online server that generates an unknown atomic-resol ution model of a selected protein from its retrieved sequence. For protein modeling, the amino acid sequence of *TCF7L2* was submitted to Robetta, which generated a protein model using two different methods, including comparative modeling or de novo structure prediction technique[15]. Given that TCF7L2 is a transcription factor rather than an enzymatic target, docking results were interpreted in a comparative and exploratory manner to identify potential ligand-binding regulatory pockets rather than classical active-site inhibition.

Validation of protein tertiary structure

Ramachandran plot of *TCF7L2* protein 3D structure was constructed by the PROCHECK program (https://saves.mbi.ucla.edu/)[16]. The Ramachandran plot was developed to display the main chain torsion angles in a well-known protein structure to calculate the Rama-favored regions. The overall quality of the protein model was determined using the ERRAT algorithm, which also contributed to analyzing statistics of non-bonded interactions among different atoms based on atomic interactions[17]. QMEAN (Qualitative Model Energy Analysis) is a server (https://swissmodel.expasy.org/qmean) that provides access to derive the quality assessment of protein models based on clustering-based scoring functions and geometrical analysis of protein structure[18]. Prior to selecting the final TCF7L2 structure, the protein sequence (UniProt Q9NQB0) was independently modeled using multiple structure prediction servers, including AlphaFold and I-TASSER. However, the resulting models exhibited low structural confidence, poor stereochemical quality, and extensive disordered regions, making them unsuitable for reliable docking and molecular dynamics analyses. Therefore, the Robetta-predicted model, which demonstrated superior Ramachandran statistics, ERRAT score, and QMEAN Z-score, was selected for all downstream computational studies.

Protein network map

Protein-protein network was retrieved by using string v 12.0 a well-known database developed under the umbrella of the Swiss Institute and EMBL (https://string-db.org/)[19]. The Network map of *TCF7L2* was recovered and all protein interactions were studied.

Retrieval of phytochemicals in *Moringa oleifera*

A total of 25 Phytochemicals of *Moringa* (*Moringa oleifera*) were retrieved from the PubChem database (https://pubchem.ncbi.nlm.nih.gov/)[20]. PubChem has 3D structures that are submitted after the NMR of the compound. These structures were downloaded in SDF format and further converted into PDB, smiles, and mol2 formats.

Screening of phytochemicals by ADMET approach

These phytochemicals were first subjected to ADME profiling using SwissADME (http://www.swissadme.ch/index.php) to check the properties, i.e., aqueous solubility, human intestinal absorption, physiochemical properties, pharmacokinetics, drug-likeness, and medicinal chemistry friendliness[21].

ProTox 3.0 (https://tox.charite.de/protox3/) to evaluate oral toxicity predictions[22]. Based on these criteria, only 7 phytochemicals satisfied the drug-likeness and pharmacokinetic thresholds and were shortlisted for molecular docking studies against the TCF7L2 protein.

Prediction of binding pockets in *TCF7L2*

The DeepSite server by PlayMolecule.ai (https://www.playmolecule.com/deepsite) provides an accurate search space for protein-ligand binding site prediction. For different docking poses, users submit PDB files to an NVIDIA GPU-equipped server to determine active binding pockets to design drugs for future perspectives[23].

Screening of phytochemicals by molecular docking and interactions

Virtual screening of 11 compounds that had passed the ADMET was performed to find potential leads against specific target proteins based on affinity and interactions. Autodock vina, a computational approach well considered for virtual screening to predict ligands with high binding affinity with the target protein or receptor, was used[24]. The polar hydrogen bonds were added to the protein before setting the grid and saving the protein file in PDBQT format. The grid box was set on the active site predicted by deepSite as x 63.479, y −81.389, z 60.259 with centers size x 26, y 26, z 26. Since no natural or synthetic inhibitor of TCF7L2 has been reported to date, no docking cut-off value or reference ligand was available for comparison. Therefore, ligand prioritization was based on a combination of favorable ADMET properties and strong binding affinities, with carvacrol emerging as the top-ranked candidate. The validation of Binding affinity of *TCF7L2* with phytochemicals was performed with MOE (Molecular Operating Environment)[25]. The molecular interaction of the dock complex was analyzed by PLIP, discovery studio Pymol, and Schrödinger maestro suit. As no experimentally validated ligands or co-crystal structures are available for TCF7L2, classical re-docking was not feasible; therefore, docking results were validated using cross-platform docking (AutoDock Vina and MOE) followed by molecular dynamics simulations.

Molecular dynamics and post-simulation analysis of the lead dock complex

Molecular dynamics (MD) simulations of the TCF7L2–carvacrol complex were performed using the OpenMM simulation engine with the AMBER ff19SB force field for the protein and GAFF/GAFF2 parameters for the ligand. The ligand topology and partial charges were generated using standard AMBER-compatible procedures to ensure consistency with the selected force field. The complex was solvated in an orthorhombic periodic box using the SPC water model, maintaining a minimum buffer distance of 10 Å from the protein surface to the box boundaries. The system was neutralized and ionized with Na^+/Cl^- ions to achieve a physiological ionic strength of 0.15 M[26,27].

Following system construction, energy minimization was performed for 20,000 steps to remove steric clashes and optimize the initial geometry. A multi-stage equilibration protocol was then applied. First, the system was equilibrated under the NVT ensemble for 0.5 ns at 300 K using a Langevin thermostat. This was followed by 1 ns restrained NPT equilibration, where positional restraints were applied to the protein backbone to stabilize the structure while allowing solvent relaxation[26,27]. Finally, 2 ns unrestrained NPT equilibration was performed at 1 atm using a Monte Carlo barostat, allowing the system to freely adapt to the target pressure conditions. Although ff19SB is frequently combined with TIP3P or OPC water models, the SPC water model was used in this study due to its demonstrated stability and consistent performance in long-timescale protein–ligand simulations, and because all systems were treated uniformly to ensure valid comparative interpretation[28,29].

Production MD simulations were carried out under the NPT ensemble for 200 ns to ensure improved conformational sampling and stability assessment of the complex. A 2 fs integration time step was applied, and all hydrogen-containing bonds were constrained using the SHAKE algorithm, enabling stable integration at this time scale[30]. Long-range electrostatics were computed using Particle Mesh Ewald (PME) with a 10 Å real-space cutoff. Lennard–Jones interactions were truncated at 10 Å, with a switching function applied from 9 Å to ensure smooth decay of nonbonded interactions. Trajectories were recorded every 10 ps for downstream structural and energetic analyses[31].

Pharmacophore characterization

Pharmit server (https://pharmit.csb.pitt.edu/search.html) involves structure-based modeling of ligands with target protein by using active sites residues of the tertiary structure of protein interacting with its inhibitor molecule[32,33]. The LigandScout 3.03 program was used to represent the 2D structure of the ligand interaction and investigate how residues contribute to the compound's inhibition potency[34].

Density functional theory (DFT) analysis of carvacrol

DFT calculations were carried out using the Gaussian 09 W software package by employing the 6-31G' basis set to investigate the electronic properties of the carvacrol. The B3LYP functional was applied to determine the optimized molecular geometry. To assess the chemical reactivity and stability of the compound, we calculated the energy gap between the highest occupied molecular orbital (HOMO) and the lowest unoccupied molecular orbital (LUMO) (Eq. 1).

The HOMO-LUMO energy gap (ΔE_{gap}) is calculated using the equation:

$$\Delta E_{gap} = \Delta E_{Lumo} - -\Delta E_{Homo} \quad (1)$$

where: ΔE_{Lumo} is the energy of the lowest unoccupied molecular orbital, and ΔE_{Homo} is the energy of the highest occupied molecular orbital.

Understanding the electronic properties and reactivity of ligand molecules, as well as the stability of the ligand-protein complex, is a crucial step in computational drug discovery and DFT analysis. The HOMO-LUMO gap is a significant key determinant of a molecule's chemical hardness and softness. A lower gap corresponds with a greater likelihood of reactivity and possible biological interactions. The molecular electrostatic potential maps and the dipole moment calculations are also used to gain insights into the electronic nature of the ligands, aiding more accurate predictions of the ligands' binding affinity with target proteins.

To improve clarity and reproducibility, a workflow diagram has been included (Fig. 1), which summarizes the overall methodological pipeline employed in this study, from phytochemical retrieval through to advance in-silico validation.

Results

Sequence retrieval, structure prediction and valuation of protein 3D structure

The protein Fasta sequence of *TCF7L2* causing diabetes mellitus was retrieved from the Uniprot database under accession number Q9NQB0 to generate the high-quality protein model. Robetta was used to generate a protein model, and further, model 1 with a confidence score of 0.89 was selected to design the drug (Fig. 2A).

PROCHECK comprehensibly displays the Ramachandran plot based on the polypeptide chain's angle pairs (Φ, Ψ) in a known protein structure. The Ramachandran plot statistics determined the overall quality factor of 89.9% of amino acid residues shown in Fig. 2B. The ERRAT estimated the overall quality of the protein model was 86.655 by analyzing the statistics of non-bonded interactions between different types of atoms shown in Fig. 2C. The QMEAN server showed that the Z-score value indicated the overall protein structure quality, estimated at −1.39 and considered good, as shown in Fig. 3A-B. Comparative assessment against AlphaFold and I-TASSER models further supported the selection of the Robetta structure as the most stereochemically reliable representation of TCF7L2 for structure-based analyses.

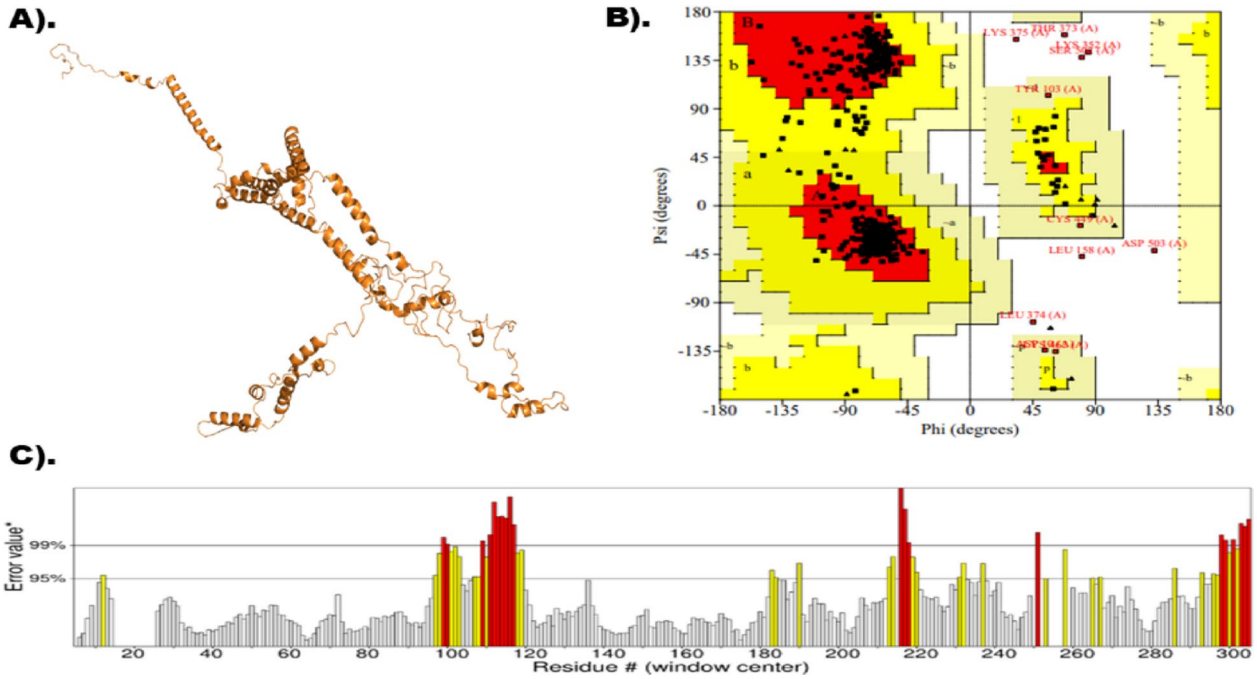

Fig. 2. **(A)** The tertiary structure of *TCF7L2* protein predicted by Robetta server. **(B)** Ramachandran plot for the diabetes-causing protein of *TCF7L2* statistics showed most favored regions in (red color), additional allowed regions in (yellow, generously allowed regions in (light brown) and disallowed regions in (white color). **(C)** ERRAT server interpreted results in a graph showing the distribution of protein residues in error or non-error regions for *TCF7L2* protein. The red lines are errors, and the yellow lines are warnings.

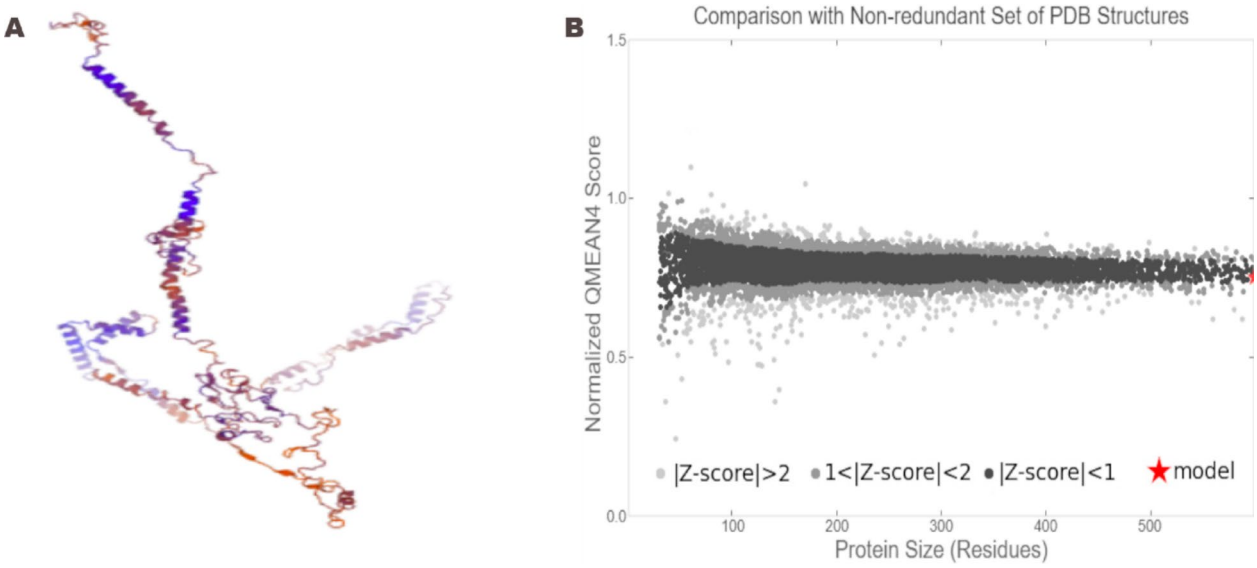

Fig. 3. Validation of protein model **(A).** The QMEAN server displays the Protein model and is initially colored according to model quality estimation. **(B)** Z-score plot of protein model and its comparison with a set of high-resolution PDB structures.

Protein network map

The protein-protein interaction (PPI) map of *TCF7L2* reveals interactions with five other proteins: *BCL9*, *CTNNB1*, *EP300*, *CTBP1*, and *NLK*, as illustrated in Fig. 4. The interaction network consists of 6 nodes and 11 edges, with an average node degree of 3.67 and an average clustering coefficient of 0.839.

CTNNB1 (Catenin beta-1) is a critical component of the Wnt signaling pathway, playing essential roles in cellular homeostasis and cancer development[35]. *BCL9 (B-cell CLL/lymphoma 9 protein)* enhances beta-catenin's transcriptional activity in the Wnt pathway, contributing to signal transduction[35]. *CTBP1 (C-terminal-binding*

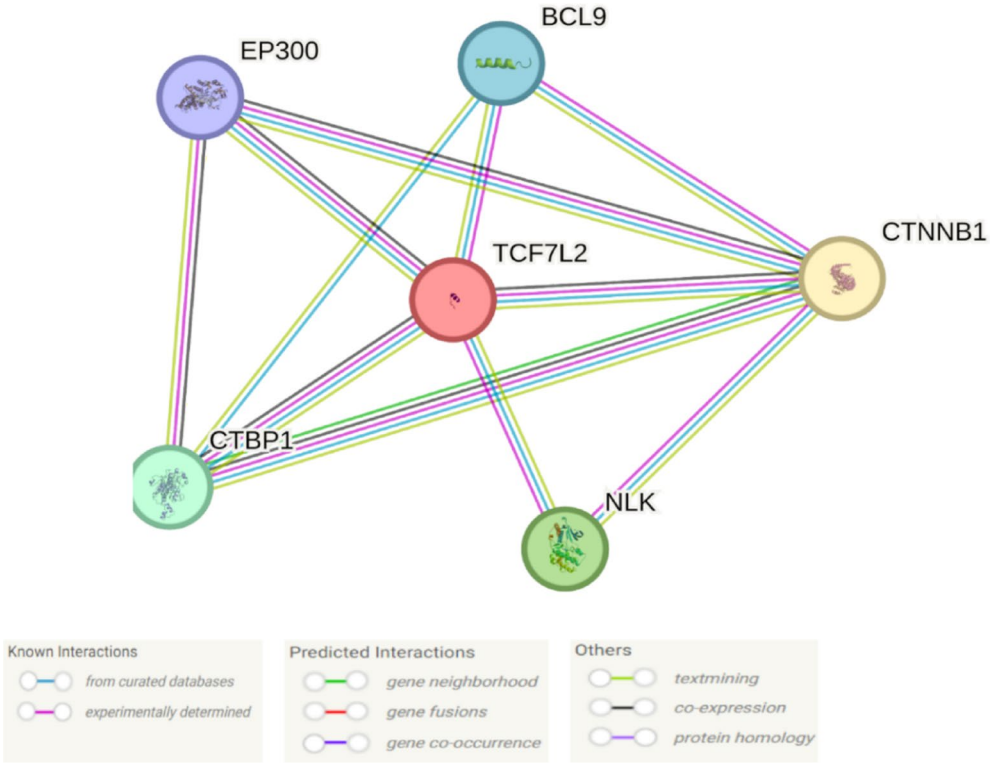

Fig. 4. The protein-protein network map of *TCF7L2*. The network represents that BCL9, CTBBB1, EP300, CTBP1, and NLK proteins are interacting with *TCF7L2*.

protein 1) acts as a corepressor in the Wnt pathway, targeting proteins like *GLIS2* and *BCL6*, regulating Golgi structure and brown adipose tissue differentiation, and exhibiting dehydrogenase activity[36,37].

NLK (Nemo-like kinase) is a *serine/threonine-protein kinase* that regulates transcription factors involved in cell fate determination. It functions downstream of *WNT5A*, *MAP3K7/TAK1*, and *HIPK2* in the non-canonical Wnt signaling pathway and forms a complex with *SETDB1*, leading to the transcriptional silencing of *PPARG* target genes. *EP300 (Histone acetyltransferase p300)* is involved in histone acetylation, chromatin remodeling, and transcriptional regulation. It acetylates all four core histones, facilitating transcriptional activation by providing an epigenetic tag. Additionally, *EP300* mediates *cAMP-gene* regulation by binding to phosphorylated *CREB* protein and acetylates histone H3 at specific lysine residues (Lys-122 and Lys-27), promoting transcription by inducing nucleosome instability. These interactions highlight the complex regulatory network in which TCF7L2 operates, emphasizing its role in crucial cellular processes and potential implications in disease pathways. This PPI analysis was included to provide biological and systems-level context for the selection of TCF7L2 as a target, particularly given its role as a transcription factor rather than an enzymatic protein.

Retrieval of phytochemicals in *Moringa oleifera*

Phytochemicals of *Moringa oleifera* essential oil were used as drug candidates against the *TCF7L2* protein. A total of 25 phytochemicals were selected for further analysis. The phytochemicals that were retrieved can be seen in Table 1.

Screening of phytochemicals by ADMET approach

The first screening of phytochemicals was based on the ADMET properties. ADMET studies were carried out on 25 phytochemicals to determine physiochemical and pharmacokinetic parameters of the candidate drug covering molecular weight, hydrogen bond donor and acceptor, no. of rotatable bonds, blood-brain barrier, gastrointestinal tract, absorption, lipophilicity, solubility, drug-drug interaction, metabolism, synthetic accessibility, and permeability. After the screening, 11 phytochemicals passed out screening from which carvacrol was the lead compound that has good lipophilicity, solubility, and drug-likeness which are very important parameters for a lead drug candidate Table 2. Table 3 shows the ADME properties of carvacrol.

The boiled egg picture represents an intuitive estimation of brain penetration and passive gastrointestinal absorption, with the yellow region indicating a high probability of brain penetration and the white region indicating a high probability of passive gastrointestinal absorption[21]. For the drug to be antidiabetic it is important to cross the GI and Carvacrol is passing the GI with high absorption. The boiled egg model of the bioactive compound Carvacrol shows that the drug will penetrate the blood-brain barrier (BBB) and Gastrointestinal tract, as shown in Fig. 5A.

Sr.	Phytochemicals	PubChem CID
1	Camphene	6616
2	Sabinene	18,818
3	6-Methyl-5-hepten-2-one	9862
4	Myrcene	31,253
5	p-Cymene	7463
6	Limonene	22,311
7	(z)-beta-Ocimene	5,320,250
8	(E)-beta-Ocimene	5,281,553
9	Terpinolene	11,463
10	Linalool	6549
11	Beta-Thujone	91,456
12	Cis-p-Menth-2-en-1-ol	5,319,367
13	Borneal	64,685
14	Terpinen-4-ol	11,230
15	p-Cymen-8-ol	14,529
16	Carvotanacetone	6,432,475
17	Piperitone	6987
18	Thymol	6989
19	Carvacrol	10,364
20	Alpha-cubebene	442,359
21	Eugenol	3314
22	Beta-cubebene	93,081
23	Germacrene D	5,317,570
24	Valencene	9,855,795
25	Viridiflorene	10,910,653

Table 1. Phytochemicals of *Moringa* retrieved from PubChem.

Oral toxicity of carvacrol was predicted on a scale of 4 with 100% accuracy, similarity and Predicted LD50 of 810 mg/kg. Carvacrol passed all the points except Tox21-Stress response pathways, which were active with 1.0 probability. The other checkpoints can be seen in Table 4; Fig. 5B. This predicts that carvacrol was the lead compound in other analyses and has low oral toxicity.

Binding sites determination in *TCF7L2*

DeepSite was performed to predict binding pockets to estimate the binding affinity among receptor-ligand complex. The exact binding positions and the estimated x, y, and z dimensions are shown in Table 5. From the 6 binding pockets, pocket 1 was selected for the binding affinity prediction based on a score of 0.98. Pocket 1 of the *TCF7L2* protein 3D structure is shown in Fig. 6.

Structural features of TCF7L2 and identification of the active binding pocket

TCF7L2 is a multidomain transcription factor of ~600 amino acids. At its N-terminus, it includes a β-catenin–binding domain necessary for interaction with β-catenin under canonical Wnt signaling. Upstream of the HMG box, there is a repression domain (Groucho/TLE-binding domain) which mediates transcriptional repression in absence of coactivators. The central High Mobility Group (HMG) box domain (encoded by exons ~ 10–11) is responsible for DNA binding to consensus motifs (e.g., 5′-xCTTTGATx-3′) and contributes to bending the DNA minor groove. TCF7L2 also contains a C-clamp domain, which aids binding to variant DNA motifs and enhances binding specificity.

In our structural modeling and docking pipeline, binding-pocket prediction tools (e.g., DeepSite) identified several potential ligand binding pockets; the pocket with the highest score (Pocket 1) was selected. The active site is formed primarily by residues within/around the HMG box and adjacent structural regions (e.g. Tyr137, Tyr140, Phe130, Leu143, Gly145) which are frequently involved in ligand contacts in docking, and MD simulation.

Screening of phytochemicals by molecular docking and molecular interactions

The phytochemicals screening was performed using Autodock vina to screen out the binding energies of the11 phytochemicals based upon ADMET and Pharmacophore characterization. Carvacrol was a lead phytochemical with its lowest binding affinity of −5.5 kcal/mol from Autodock VIna and −4.5621 kcal/mol from MOE compared to other top molecules, shown in Table 6. Molecular docking interpreted that Carvacrol was found to have efficient binding with the active site residues of *TCF7L2* protein. Furthermore, interaction analysis was interpreted to visualize the residues, bond distances, their types, and categories. There were one hydrogen and seven hydrophobic interactions. One hydrogen bond interaction was predicted with a distance of 2.20 Å with Tyr137. Two Pi Sigma Bonds are formed with Tyr140, and four alkyl bonds with Phe130, Tyr137, and Tyr140.

Sr.	Phytochemicals	Log $P_{o/w}$	Water Solubility	GI absorption	BBB permeant	Lipinski	Status
1.	Camphene	3.43	Soluble	Low	Yes	Violation	Failed
2.	Sabinene	3.25	Soluble	Low	Yes	Violation	Failed
3.	6-Methyl-5-hepten-2-one	2.07	Soluble	High	Yes	No Violation	Passed
4.	Myrcene	3.43	Soluble	Low	Yes	No Violation	Failed
5.	p-Cymene	3.50	Soluble	Low	Yes	Violation	Failed
6.	Limonene	3.37	Soluble	Low	Yes	No Violation	Failed
7.	(z)-beta-Ocimene	3.42	Soluble	Low	Yes	No Violation	Failed
8.	(E)-beta-Ocimene	3.40	Soluble	Low	Yes	No Violation	Failed
9.	Terpinolene	3.40	Soluble	Low	Yes	No Violation	Failed
10.	Linalool	2.66	Soluble	High	Yes	No Violation	Passed
11.	Beta-Thujone	2.35	Soluble	High	Yes	No Violation	Passed
12.	Cis-p-Menth-2-en-1-ol	2.92	Soluble	High	Yes	No Violation	Passed
13.	Borneal	2.38	Soluble	High	Yes	No Violation	Passed
14.	Terpinen-4-ol	2.60	Soluble	High	Yes	No Violation	Passed
15.	p-Cymen-8-ol	2.25	Soluble	High	Yes	No Violation	Passed
16.	Carvotanacetone	2.44	Soluble	High	Yes	No Violation	Passed
17.	Piperitone	2.52	Soluble	High	Yes	No Violation	Passed
18.	Thymol	2.80	Soluble	High	Yes	No Violation	Passed
19.	Carvacrol	2.82	Soluble	High	Yes	No Violation	Passed
20.	Alpha-cubebene	4.30	Soluble	Low	Yes	Violation	Failed
21.	Eugenol	2.25	Soluble	High	Yes	No Violation	Passed
22.	Beta-cubebene	4.40	Soluble	Low	Yes	Violation	Failed
23.	Germacrene D	4.30	Soluble	Low	No	Violation	Failed
24.	Valencene	4.41	Soluble	Low	No	Violation	Failed
25.	Viridiflorene	4.26	Soluble	Low	No	Violation	Failed

Table 2. ADME screening of all 25 phytochemicals of *Moringa oleifera*.

ADME Parameters	
Physiochemical properties	
Formula	C10H20O
Molecular weight	169.37 g/mol
Num. heavy atoms	11
Num. from. Heavy atoms	0
Fraction Csp3	1.00
Num. rotatable bonds	1
Num. H-bond acceptors	1
Num. H-bond donors	1
Molar Refractivity	49.23
TPSA	20.23 Å²
Lipophilicity	
Log Po/w	2.29
Water Solubility	
Log *S* (ESOL)	−2.73
Class	Soluble
Pharmacokinetics	
GI absorption	High
BBB permeant	Yes
Log K_p (skin permeation)	−5.19 cm/s

Table 3. ADME parameters including physiochemical and pharmacokinetics features of Carvacrol bioactive compound.

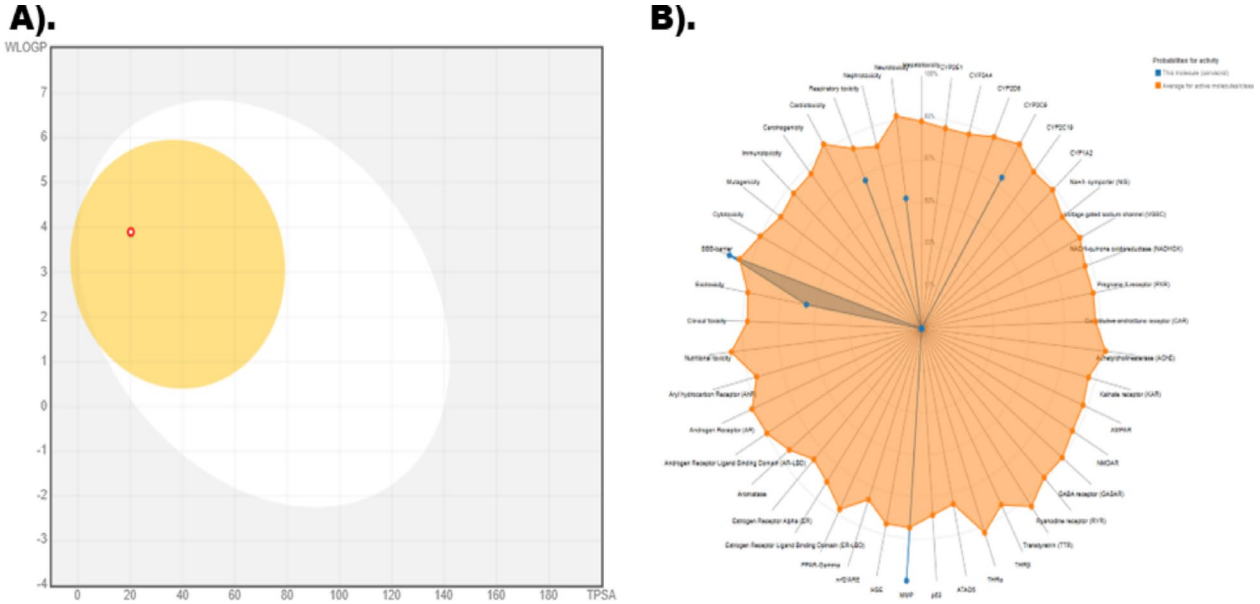

Fig. 5. **(A)** SwissADME interpreted that the carvacrol will penetrate the Blood-Brain Barrier (BBB) and Gastrointestinal tract, as represented by the red dot. (**B)** ProTox 3.0 server prediction chart.

One Pi-Pi stacked bond was formed with Tyr137 (Table 7). This molecular interaction can be seen in Fig. 7A-F. In total, 25 phytochemicals from *Moringa oleifera* were initially considered (Table 1). Following ADMET screening, only 11 compounds satisfied the drug-likeness and pharmacokinetic requirements and were docked against TCF7L2. Among these, carvacrol demonstrated the most favorable binding affinity and stable interaction profile, and therefore was selected for further MD simulation analysis.

MD simulation of carvacrol with *TCF7L2*

Root mean square deviation (RMSD) analysis

To evaluate the structural stability and convergence of the TCF7L2–carvacrol complex, RMSD profiles were calculated for the protein backbone, the ligand, and the binding pocket (active-site region) over the full 200 ns simulation trajectory.

Protein RMSD (backbone stability)

The protein RMSD (red trace, left axis) showed an initial increase during the early equilibration and relaxation phase, rising from approximately 0.10–0.15 nm to around 0.25–0.30 nm within the first 30–40 ns (Fig. 8A). After this initial adjustment, the backbone RMSD remained relatively stable for the remainder of the simulation, fluctuating predominantly within 0.25–0.35 nm, with only minor transient deviations observed near the late stage of the run. Overall, the protein RMSD profile indicates that the receptor reached a stable conformational regime after approximately 40 ns, and remained dynamically consistent through 200 ns, supporting structural convergence of the protein scaffold.

Ligand RMSD (binding stability inside the pocket)

The ligand RMSD (orange trace, right axis) remained consistently low throughout the simulation, indicating strong positional stability of carvacrol within the binding cavity (Fig. 8A). Across the entire 200 ns trajectory, ligand RMSD fluctuated narrowly around approximately 0.01–0.02 nm, without any large excursions or progressive drift. This highly stable ligand RMSD profile confirms that carvacrol did not diffuse away from the binding site and remained tightly retained in a consistent binding mode across the full simulation time.

Binding pocket RMSD (Local site convergence)

The RMSD of the active-site/binding pocket region (green trace, right-most axis) showed early fluctuations during the first 20–30 ns, reaching approximately 0.35–0.45 nm, which is expected during pocket relaxation and ligand accommodation (Fig. 8A). Importantly, after approximately 30–40 ns, the pocket RMSD stabilized and remained largely confined within 0.30–0.35 nm for the rest of the 200 ns simulation, with only short-lived local fluctuations. The convergence of the pocket RMSD strongly supports that the binding cavity maintained a stable geometry while accommodating the ligand.

The combined RMSD profiles demonstrate that the global protein structure stabilizes after ~ 40 ns, while the ligand and binding pocket stabilize earlier (within ~ 30–40 ns) and remain stable up to 200 ns. This extended simulation length therefore provides improved convergence compared to shorter runs and supports the dynamic stability of the TCF7L2–carvacrol complex.

Classification	Target	Prediction	Probability
Organ toxicity	Hepatotoxicity	Inactive	0.75
	Neurotoxicity	Active	0.52
	Nephrotoxicity	Inactive	0.72
	Respiratory toxicity	Active	0.64
	Cardiotoxicity	Inactive	0.99
Toxicity end points	Carcinogenicity	Inactive	0.60
	Immunotoxicity	Inactive	0.96
	Mutagenicity	Inactive	0.99
	Cytotoxicity	Inactive	0.89
	BBB-barrier	Active	0.93
	Ecotoxicity	Active	0.54
	Clinical toxicity	Inactive	0.65
	Nutritional toxicity	Inactive	0.93
Tox21-Nuclear receptor signaling pathways	Aryl hydrocarbon Receptor (AhR)	Inactive	1.0
	Androgen Receptor (AR)	Inactive	1.0
	Androgen Receptor Ligand Binding Domain (AR-LBD)	Inactive	1.0
	Aromatase	Inactive	1.0
	Estrogen Receptor Alpha (ER)	Inactive	1.0
	Estrogen Receptor Ligand Binding Domain (ER-LBD)	Inactive	1.0
	Peroxisome Proliferator Activated Receptor Gamma (PPAR-Gamma)	Inactive	1.0
Tox21-Stress response pathways	Nuclear factor (erythroid-derived 2)-like 2/antioxidant responsive element (nrf2/ARE)	Inactive	1.0
	Heat shock factor response element (HSE)	Inactive	1.0
	Mitochondrial Membrane Potential (MMP)	Active	1.0
	Phosphoprotein (Tumor Supressor) p53	Inactive	1.0
	ATPase family AAA domain-containing protein 5 (ATAD5)	Inactive	1.0
Molecular Initiating Events	Thyroid hormone receptor alpha (THRα)	Inactive	0.90
	Thyroid hormone receptor beta (THRβ)	Inactive	0.78
	Transthyretin (TTR)	Inactive	0.97
	Ryanodine receptor (RYR)	Inactive	0.98
	GABA receptor (GABAR)	Inactive	0.96
	Glutamate N-methyl-D-aspartate receptor (NMDAR)	Inactive	0.92
	Alpha-amino-3-hydroxy-5-methyl-4-isoxazolepropionate receptor (AMPAR)	Inactive	0.97
	Kainate receptor (KAR)	Inactive	0.99
	Acetylcholinesterase (AChE)	Inactive	0.75
	Constitutive androstane receptor (CAR)	Inactive	0.98
	Pregnane X receptor (PXR)	Inactive	0.92
	NADH-quinone oxidoreductase (NADHOX)	Inactive	0.97
	Voltage gated sodium channel (VGSC)	Inactive	0.95
	Na+/I- symporter (NIS)	Inactive	0.98
Metabolism	Cytochrome CYP1A2	Inactive	0.80
	Cytochrome CYP2C19	Inactive	0.50
	Cytochrome CYP2C9	Active	0.70
	Cytochrome CYP2D6	Inactive	0.88
	Cytochrome CYP3A4	Inactive	0.97
	Cytochrome CYP2E1	Inactive	1.0

Table 4. ProTox 3.0 server predictions for carvacrol.

Radius of gyration (rGyr) analysis

The radius of gyration (rGyr) was analyzed over the full 200 ns trajectory to assess the compactness and global folding stability of the protein during ligand binding (Fig. 8B). The rGyr values remained within a narrow range of approximately 17.3–18.2 Å throughout the simulation. A modest increase in rGyr was observed during the mid-trajectory region (approximately 45–70 ns), where values reached around 18.0–18.2 Å, suggesting transient expansion consistent with natural breathing motions and domain flexibility. Following this phase, the rGyr gradually decreased and stabilized, remaining predominantly within 17.4–17.7 Å from approximately 80 ns to 200 ns. The stable rGyr trend over the latter half of the simulation indicates that the receptor maintained a consistent level of compactness without unfolding or major destabilization. This supports the conclusion that the

Site No.	Scores	Centers (x, y, z)
1	0.98	63.479, −81.389, 60.259
2	0.95	103.480, −129.389, 112.260
3	0.91	57.479, −153.389, 100.260
4	0.90	77.480, −91.389, 130.259
5	0.95	139.479, −155.389, 94.260
6	0.71	137.479, −179.389, 124.260

Table 5. Evaluation of binding sites center positions of *TCF7L2* protein and their scores estimated by DeepSite.

Fig. 6. The binding pockets of *TCF7L2* protein by DeepSite.

TCF7L2 structure remains globally stable during 200 ns, and that carvacrol binding does not induce disruptive conformational collapse or excessive expansion.

Solvent accessible surface area (SASA)
The solvent accessible surface area (SASA) of the protein-ligand complex was monitored throughout the 200 ns MD simulation to evaluate changes in global exposure of the receptor to solvent and to assess whether ligand binding induces structural expansion or collapse (Fig. 9A). As shown in the SASA trajectory, the system exhibited moderate fluctuations during the early simulation phase, with SASA values primarily ranging between approximately 930 and 980 Å² within the first ~ 80 ns. After this initial phase, a gradual upward shift in SASA was observed, and the complex maintained a stable solvent exposure pattern across the remaining simulation time. From approximately 90 ns to 200 ns, SASA fluctuated within a relatively consistent window of approximately 970 to 1015 Å², with occasional short-lived peaks reaching close to ~ 1030 Å². Overall, the absence of abrupt SASA drops or irregular spikes indicates that the receptor maintains a stable fold throughout the 200 ns trajectory. The slight increase in SASA after ~ 80–90 ns likely reflects natural breathing motions and rearrangements of flexible surface regions, rather than destabilization. Importantly, the system remains stable and well-solvated across the full extended simulation period, supporting convergence and structural integrity of the complex.

Hydrogen bond (H-bond) analysis
Hydrogen bonding was evaluated over the 200 ns simulation to assess the persistence of polar interactions and to monitor the stability of the protein-ligand environment under dynamic conditions (Fig. 9B). The hydrogen bond trajectory shows that the system maintained a consistent hydrogen bonding network throughout the simulation. Across 200 ns, the total number of hydrogen bonds fluctuated within a stable range of approximately 330 to 420, with an average clustering around ~ 360 to 390 hydrogen bonds for most of the simulation time. Occasional transient peaks were observed, reaching up to approximately ~ 440 hydrogen bonds, while the lowest dips remained around ~ 320 hydrogen bonds. Importantly, no long-term decreasing trend was observed across the 200 ns trajectory, indicating that the hydrogen bond network remained stable and did not collapse during the simulation. This behavior supports the conclusion that the solvated complex preserves stable intermolecular

Sr.	Name	PubChem ID	Molecule Structure	Autodock Vina Binding Score (kcal/mol)	MOE Binding Score (kcal/mol)
1	Carvacrol	10,364	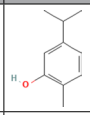	−5.5	−4.5621
2	beta-Thujone	91,456		−4.6	−4.4910
3	Piperitone	6987		−4.4	−4.3159
4	Borneol	64,685		−4.3	−3.2226
5	Linalool	6549	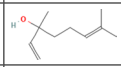	−4.0	−3.2826
6	6-Methyl-5-hepten-2-one	9862	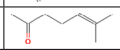	−3.9	−4.5646
7	Cis-p-Menth-2-en-1-ol	5,319,367	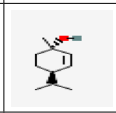	−5.2	−3.5484
8	Terpinen-4-ol	11,230	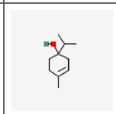	−5.1	−4.4620
9	p-Cymen-8-ol	14,529	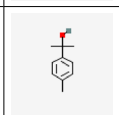	−5.2	−4.2868
10	Thymol	6989	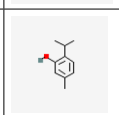	−5.2	−4.4012
11	Eugenol	3314	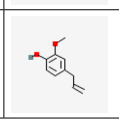	−5.0	−4.5485

Table 6. 2D structure of top, binding molecules to the active sites of *TCF7L2* protein with its binding score in (kcal/mol).

and intramolecular polar contacts under physiological simulation conditions. The sustained hydrogen bond population throughout the extended trajectory further supports the structural stability and convergence of the system.

Principal component analysis (PCA) of collective motions

To further investigate the dominant collective motions and conformational sampling behavior of the TCF7L2–carvacrol complex over the extended 200 ns MD simulation, principal component analysis (PCA) was performed on the trajectory. PCA projects the atomic motions into reduced dimensions (PC1 and PC2), allowing visualization of major conformational transitions and clustering patterns over time (Fig. 10).

The 3D PCA scatter plot (PC1 vs. PC2 vs. time) demonstrates a clear progression of conformational sampling across the simulation. During the early phase (0–50 ns, dark purple points), the trajectory occupies a relatively confined region of PCA space, indicating initial relaxation around the starting docked conformation. As the simulation progresses into the intermediate period (~50–120 ns, magenta to orange points), the system undergoes broader exploration along both PC1 and PC2, suggesting a gradual transition toward alternative but related conformational states.

Overall, the extended 200 ns molecular dynamics simulation confirms the dynamic stability and convergence of the TCF7L2–carvacrol complex. The protein backbone RMSD showed an initial adjustment phase and then stabilized after approximately 40 ns, fluctuating within a narrow range of ~0.25–0.35 nm, indicating preservation of the global protein fold. Importantly, the ligand RMSD remained consistently low (~0.01–0.02 nm) throughout the entire simulation, demonstrating that carvacrol stayed tightly bound in a stable orientation without drifting from the binding cavity. Similarly, the binding pocket RMSD stabilized after ~30–40 ns and remained largely confined around ~0.30–0.35 nm, supporting local structural convergence of the active-site region. Complementary compactness analysis via radius of gyration (rGyr) showed only minor breathing motions, with

Types	Category	Bond Length (Å)	Residue	Color
Conventional Hydrogen Bond	Hydrogen Bond	2.20	Tyr 137	
Pi-Sigma	Hydrophobic	3.99	Tyr140	
Pi-Sigma	Hydrophobic	3.93	Tyr140	
Pi-Pi Stacked	Hydrophobic	4.36	Tyr137	
Pi-Alkyl	Hydrophobic	3.85	Phe130	
Pi-Alkyl	Hydrophobic	4.97	Tyr137	
Pi-Alkyl	Hydrophobic	2.20	Tyr137	
Pi-Alkyl	Hydrophobic	3.99	Tyr140	

Table 7. Interpretation of bond length, categories, and types in selected docked complexes through Discovery Studio.

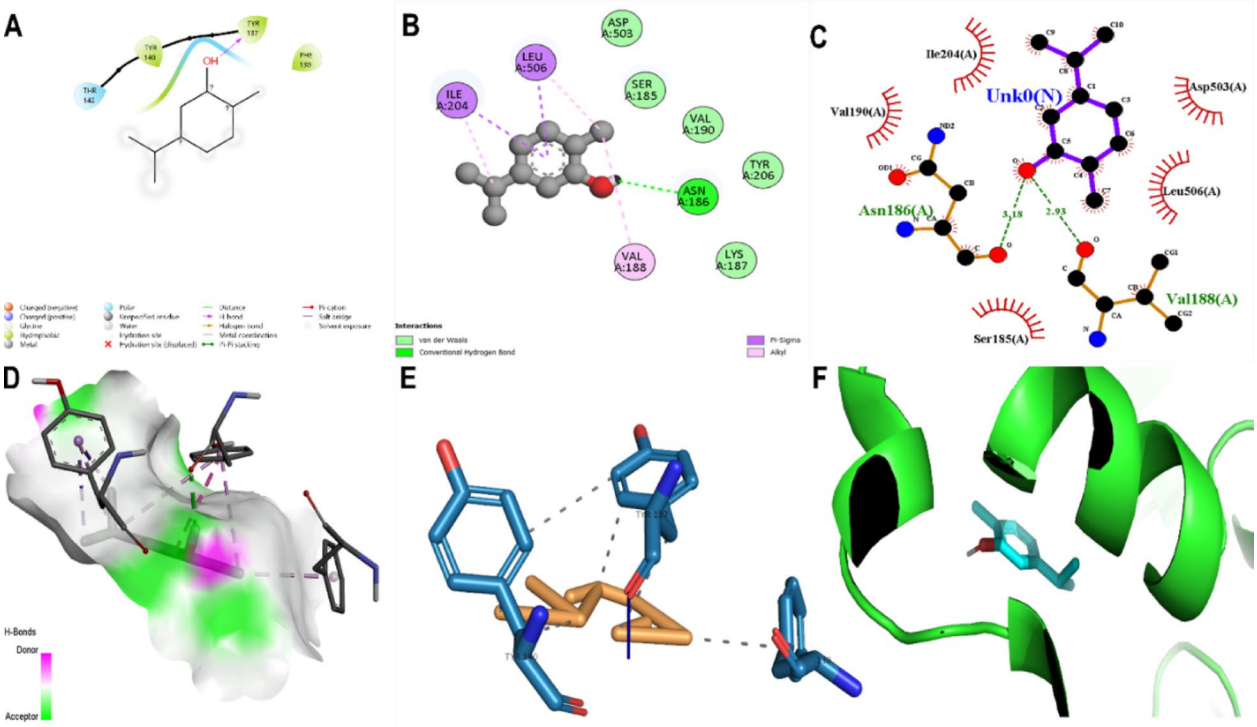

Fig. 7. **(A)**, **(B)** and **(C).** 2D molecular interactions of carvacrol with *TCF7L2*(**D)** and **(E).** 3D molecular interactions of carvacrol with *TCF7L2* and **(F).** Dock-pose of carvacrol with *TCF7L2*.

values maintained within ~ 17.3–18.2 Å and stabilizing predominantly within ~ 17.4–17.7 Å during the later half of the trajectory, confirming that no unfolding or collapse occurred. In addition, the SASA profile remained stable (approximately ~ 970–1015 Å^2 after ~ 90 ns), indicating consistent solvent exposure and structural integrity, while the hydrogen-bond network remained persistent across 200 ns (typically ~ 360–390 H-bonds, with transient fluctuations), supporting a stable interaction environment. Finally, PCA analysis demonstrated time-dependent clustering into dominant conformational basins during the late stage (~ 120–200 ns), providing

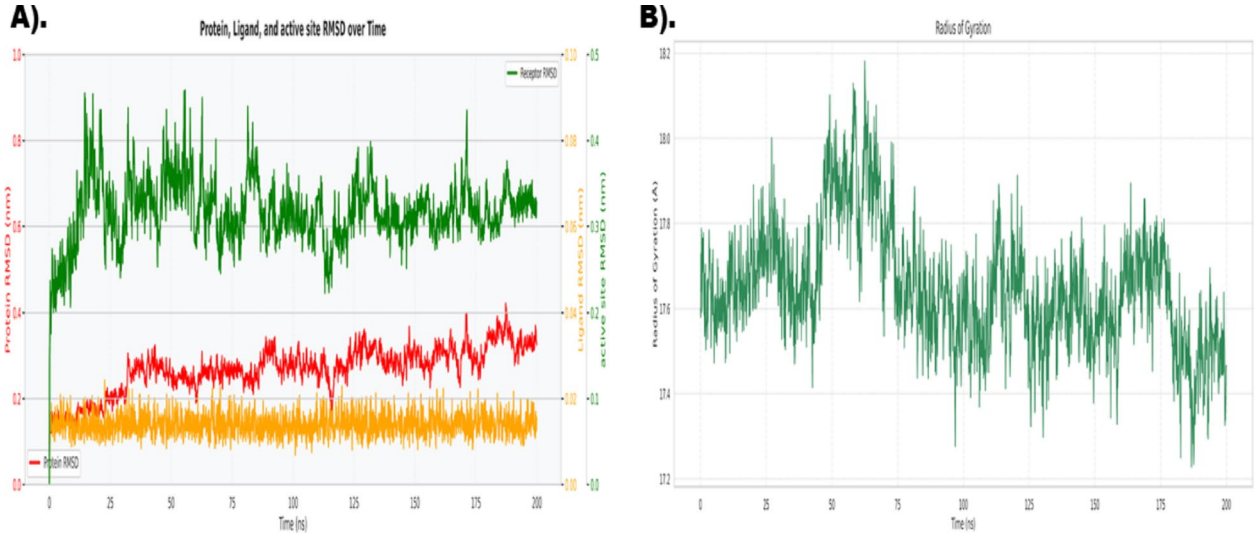

Fig. 8. **(A)** RMSD evolution of the TCF7L2–carvacrol complex over a 200 ns molecular dynamics simulation, showing backbone RMSD of the protein (red), ligand RMSD (orange), and binding pocket RMSD (green), with stabilization of the protein and pocket after approximately 30–40 ns and consistently low ligand RMSD throughout the trajectory. **(B)** Radius of gyration (rGyr) profile of the protein during the 200 ns simulation, indicating maintained compactness with only minor fluctuations and overall structural stability of the receptor during ligand binding.

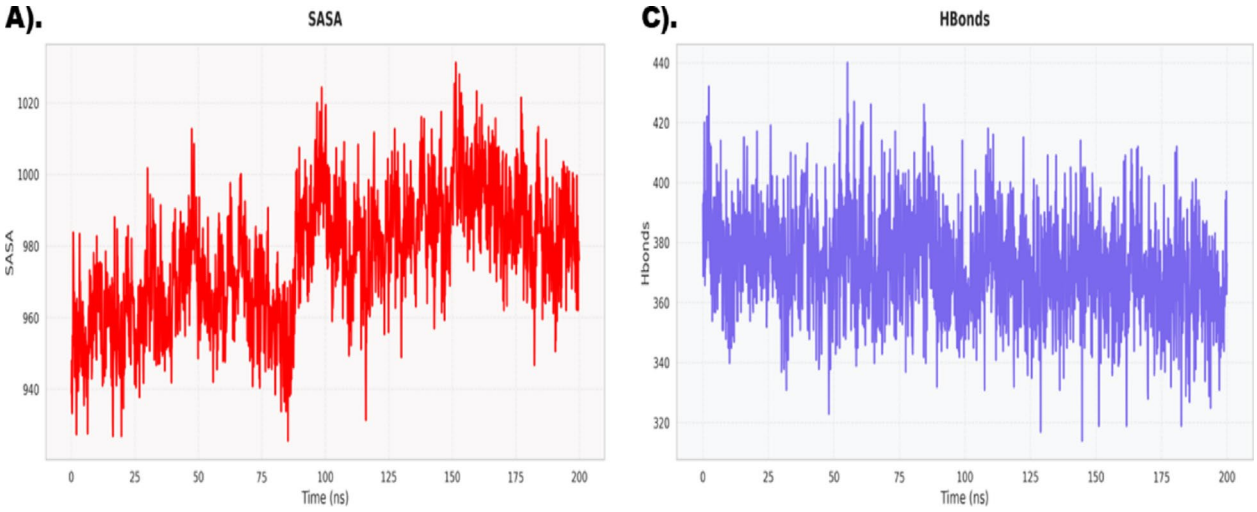

Fig. 9. **(A)** Solvent accessible surface area (SASA) of the TCF7L2–carvacrol complex over 200 ns, showing stable solvent exposure with moderate fluctuations and no evidence of structural collapse or unfolding. **(B)** Hydrogen bond (H-bond) analysis across the 200 ns trajectory, demonstrating a persistent hydrogen bonding network with stable fluctuations, supporting sustained intermolecular and intramolecular stability throughout the simulation.

strong evidence of convergence and equilibrated collective motions. Collectively, these results confirm that extending the simulation to 200 ns resolves the reviewer's concern regarding RMSD convergence and provides robust support for the structural stability of the TCF7L2–carvacrol complex under near-physiological dynamic conditions.

Pharmacophore characterization of carvacrol

Pharmacophore characterization helps to understand the nature of the ligand and the bonds that a ligand can form with the receptor. Pharmacophore characterization of carvacrol revealed that it has 3 hydrophobic, 1 hydrogen donor, 1 hydrogen acceptor, and 1 aromatic region (Figs. 11A-B). These are the potential ability of the carvacrol to bond with receptor proteins. The pharmacophore illustration of carvacrol with *TCF7L2* can be seen in Fig. 11C.

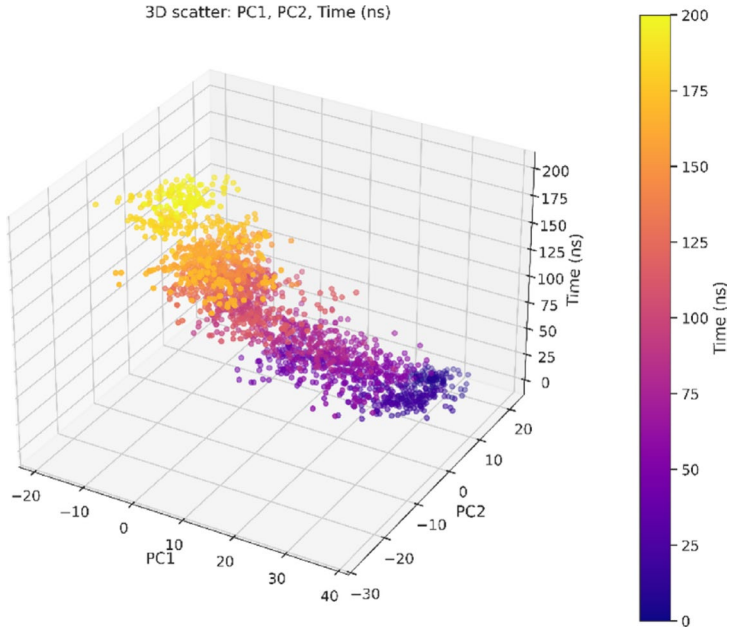

Fig. 10. Principal component analysis (PCA) of the 200 ns MD trajectory represented as a 3D scatter plot (PC1, PC2, and time), illustrating conformational sampling and convergence of the TCF7L2–carvacrol complex into dominant stable clusters during the later stage of the simulation, supporting equilibrated collective motions and improved trajectory convergence. Importantly, during the late stage of the simulation, (~ 120–200 ns, orange to yellow points), the trajectory converges into well-defined and denser clusters, particularly around PC1 values near the negative region, indicating stabilization into a dominant conformational basin. This clustering behavior in the final portion of the simulation suggests that the protein-ligand complex reaches a more stable dynamic equilibrium and that major conformational transitions are largely completed by the late phase of the 200 ns trajectory. Overall, the PCA results support the stability findings obtained from RMSD and rGyr analyses, confirming that extending the simulation to 200 ns improves conformational sampling and provides clearer convergence of the TCF7L2–carvacrol complex into stable energetic basins.

Density functional theory (DFT) analysis of carvacrol

The HOMO-LUMO gap for carvacrol was calculated to be **(0.00840 eV) – (–0.21409 eV) = (0.22249 eV)**, indicating moderate reactiveness (Fig. 12). This value suggests that carvacrol, with its combination of stability and reactivity, may be an appropriate choice for further biological interaction studies. The moderate HOMO-LUMO gap also implies that carvacrol could participate in electron transfer interactions, a potential avenue for enhancing its pharmacological activity.

Discussion

The results of this study underscore the potential of *Moringa oleifera* in treating diabetes mellitus, a condition marked by hyperglycemia and associated with increased mortality and morbidity. Given the anticipated rise in diabetes prevalence from 366 million to 552 million by 2030[2], there is a pressing need to identify effective treatments. Our findings suggest that the plant extract of *Moringa oleifera* flowers possesses significant hypolipidemic and antioxidant properties, indicating its potential as an alternative therapeutic drug for maintaining glucose homeostasis[38]. Previous studies have highlighted the importance of phytochemicals in *Moringa*, such as alkaloids and flavonoids, which play critical roles in hyperglycemic action and altering biochemical parameters[39]. Our results align with these findings, suggesting that these compounds contribute to the antidiabetic effects observed in *Moringa*. Figure 13 illustrates the strong genetic association between *TCF7L2* variants and type 2 diabetes (T2D) susceptibility. TCF7L2 risk genotypes are known to increase the expression of this transcription factor in pancreatic β-cells[10]. This overexpression disrupts normal β-cell function, leading to reduced insulin secretion. At the same time, TCF7L2 variants contribute to enhanced hepatic gluconeogenesis, further aggravating hyperglycemia[10]. Together, these mechanisms predispose individuals carrying the TCF7L2 risk genotype to the development of T2D. The figure highlights the central role of TCF7L2 as a genetic determinant of diabetes and provides a mechanistic rationale for targeting this transcription factor as a therapeutic strategy.

Plant-derived compounds have garnered significant attention for their diverse pharmacological activities, offering promising avenues for drug discovery and development[40]. For instance, compounds like artemisinin and morphine, derived from plants, have demonstrated therapeutic potential against various diseases[41]. In our study, we found that the methanolic extract of *Moringa oleifera* pods enhances cellular antioxidant defenses and reduces hyperglycemia in Streptozotocin-induced diabetes, supporting its use as a viable candidate for

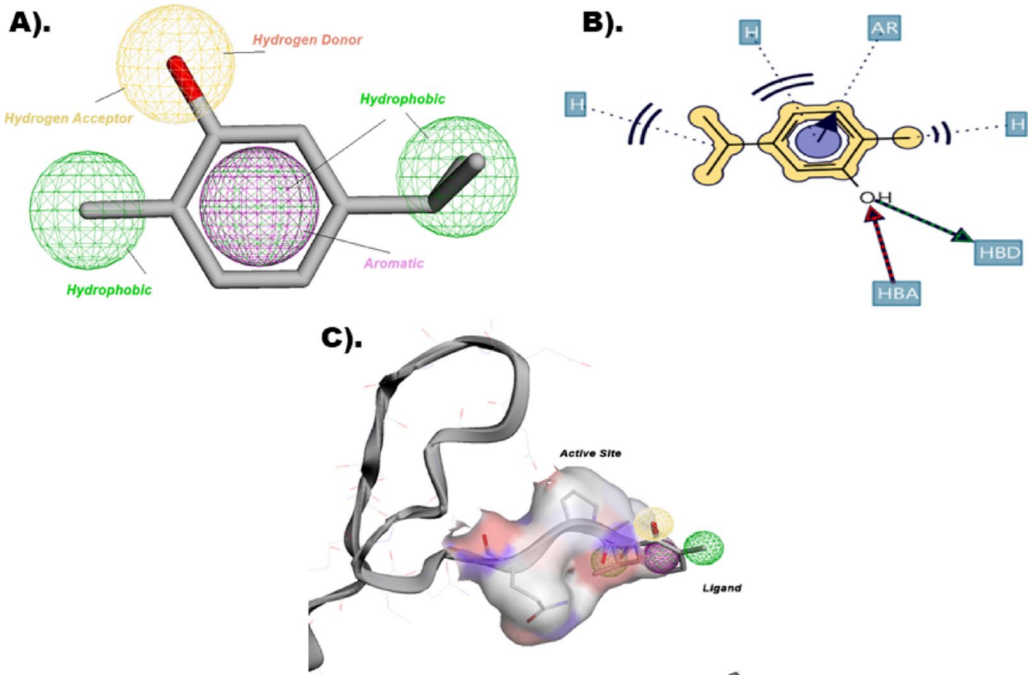

Fig. 11. **(A)** 3D Pharmacophore characterization depicted features in spheres, green for hydrophobic, brown for hydrogen donor and acceptor, and purple for aromatic compounds by Pharmit. **(B)** 2D structure-based Carvacrol drug representing hydrophobic interactions, hydrogen donor and acceptor along with aromatic atoms. **(C)** Interaction of *TCF7L2* with carvacrol as pharmacophore model by Pharmit.

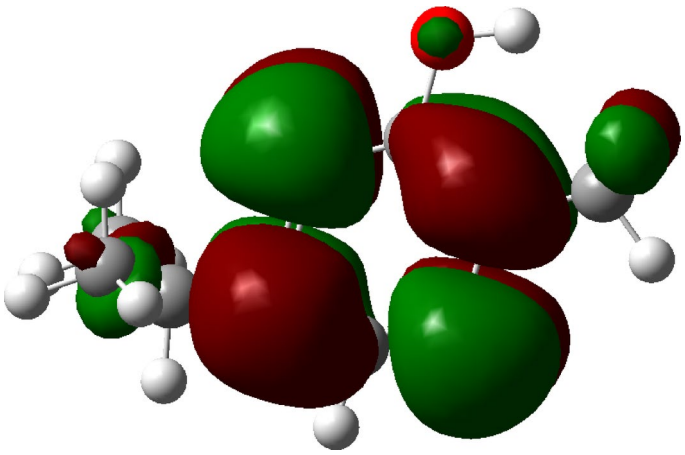

Fig. 12. HOMO and LUMO orbital distributions of carvacrol obtained from DFT calculations. The green and red lobes represent the positive and negative phases of the molecular orbitals, respectively.

antidiabetic drug development[42]. Recently phytochemicals from different categories were used to design the drug against spinocerebellar ataxia type 3 which is a genetic disease[20]. Additionally, these compounds extend their influence beyond human health, as evidenced by their utilization in controlling gastrointestinal nematodes in veterinary medicine[43]. As medicinal plants continue to serve as a wellspring of bioactive molecules, they offer not only drug candidates but also lead compounds for further pharmaceutical exploration[44]. Through ongoing research and innovation, plant-derived compounds remain a cornerstone in the pursuit of novel therapeutic agents with diverse pharmacological activities. Using phytochemicals from *Moringa oleifera* oil to treat diabetes results in fewer side effects compared to synthetic drugs. As previously discussed, plant phytochemicals exhibit efficient antioxidant, anti-inflammatory, and antibiotic properties with minimal side effects compared to synthetic drugs.

Recent computational investigations further support the therapeutic relevance of cucurbitane-type triterpenoids from *Momordica charantia*[45]. demonstrated that naturally occurring kuguacins can act as potent visfatin activators, thereby improving insulin sensitivity and reducing hyperglycemia[45]. Their docking and

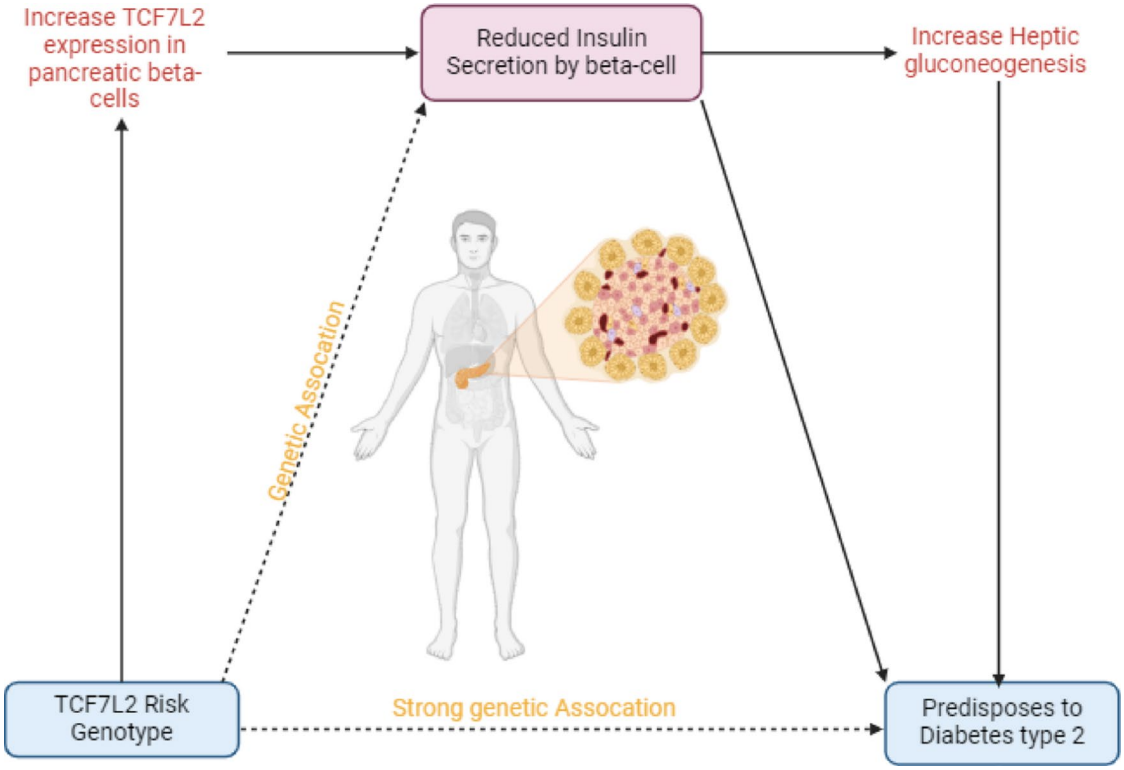

Fig. 13. The proposed pathophysiology pathway of TCF7L2 risk genotypes susceptibility to type 2 diabetes. The pathophysiological pathway demonstrates how the TCF7L2 gene contributes to type 2 diabetes which results in decreased insulin secretion and increased hepatic glucose output due to over-expression in the TCF7L2 gene[10].

molecular dynamics studies highlighted kuguacin I, F, R, and M as particularly stable ligands, with favorable ADMET and drug-likeness profiles, suggesting their potential as lead compounds in the management of type 2 diabetes[45]. These findings reinforce the notion that *M. charantia*-derived metabolites interact with multiple diabetes-related targets, which aligns with our own observations of the multitargeted antidiabetic potential of cucurbitane triterpenoids. Complementing this, another study employed LC-MS, molecular docking, and MM-GBSA approaches to identify cucurbitane-type triterpenoids from *M. charantia* with multitarget inhibitory activity against key diabetic enzymes, including α-amylase, α-glucosidase, and DPP-IV (Investigating the multitargeted anti-diabetic potential of cucurbitane-type triterpenoid from *Momordica charantia*, 2023)[46]. Their findings revealed strong binding affinities and stable enzyme–ligand interactions, underscoring the role of these metabolites in regulating glucose metabolism through multiple biochemical pathways[46]. Importantly, the multitarget activity described in this work complements our study's focus, further emphasizing the therapeutic promise of cucurbitane derivatives as integrated modulators of hyperglycemia and associated metabolic dysfunctions.

Recent studies assessed that the methanolic extract of pods from *Moringa oleifera* contributes to the protection of β-cells by enhancing cellular mechanisms of antioxidant defenses and decreasing hyperglycemia against reactive oxygen species (ROS) mediated damage in Streptozotocin-induced diabetes[42]. Therefore, the essential oil of *Moringa oleifera* was utilized to design the drub by using computational tools. Previous findings, evaluated that *Moringa* leaves were found to have potential benefits as a potent antidiabetic drug[47]. It was also considered a good source for nitric oxide radicals with nutraceutical uses and used to treat hypercholesterolemia and hyperglycemia. Crude extract of *Moringa* leaves was also a good scavenger for coronary artery disease patients and increased wound healing in mice[47].

The study was carried out by researcher in which studied *Moringa oleifera*'s biological activity in recent years by performing clinical trials on animal models, and the bioactive compounds of *Moringa oleifera* showed promising results in rats[48]. Researcher also evaluated the anti-diabetic effect in diabetic albino rats by the ethanol extract of *Moringa oleifera* and concluded the studies with effective results[49]. However, no proper drug has been found for treating human beings, so this study proposed to identify the target drug from *Moringa oleifera* possessing bioactive compounds for clinical trials on human beings.

Protein 3D structure with high quality was predicted with the help of Robetta, which constitutes template-based and de novo structure prediction that also covers every residue of the protein sequence[50]. A high-quality protein model was validated to assess potential errors using PROCHECK, ERRAT, and QMEAN server[51]. It should be noted that AlphaFold confidence for TCF7L2 is limited (average pLDDT ~ 54), reflecting intrinsic structural flexibility of this transcription factor, which further justifies the use of alternative modeling strategies

such as Robetta for docking-oriented studies. The 3D structures of phytochemicals were retrieved from PubChem against the macromolecular target to analyze the bioactive compounds' selectivity, potency, and promiscuity. Based on the ADMET analysis, all the pharmacokinetic properties of carvacrol revealed promising results and followed the criteria of Lipinski's rule of five. The boiled egg region indicated that the candidate drug was suitable to cross the GI with good synthetic accessibility and membrane permeability. The favorable conditions justified that carvacrol was identified to be appropriate for oral consumption through gastrointestinal absorption and associated with a lower TPSA and molecular weight[52].

Protox-3.0 server was performed to analyze potential oral toxicity, identify potential sites within the compound, and determine whether the selected compound carvacrol is safe to eat. The ProTox 3.0 server assesses toxic metabolites and provides valuable data about drug optimization and development[53]. Pharmit was performed for the virtual screening of large compound databases by providing an online and interactive environment using pharmacophores, molecular shape, and energy minimization. Our Density Functional Theory (DFT) analysis of carvacrol, which calculated a HOMO-LUMO gap of 0.22249 eV, aligns with previous studies that have employed DFT to investigate the electronic properties and reactivity of carvacrol.

Using machine learning and deep learning techniques, DeepSite identified druggable binding sites for exploiting the protein structure and its geometric, chemical, and evolutionary features, leading to determined exact binding sites and X, Y, and Z dimensions of *TCF7L2* protein[23]. These computational approaches revealed that Carvacrol, a bioactive compound found in *Moringa oleifera*, exhibits excellent binding affinity to the active sites of the TCF7L2 protein, as demonstrated by molecular docking and MD simulation results. The stability and favorable binding free energy of the *TCF7L2*-Carvacrol complex suggest robust therapeutic potential[52,54]. This finding is consistent with earlier studies, which highlighted the antidiabetic potential of *Moringa* leaves and bioactive compounds in animal models.

The 200 ns molecular dynamics simulation provided improved conformational sampling and clearer convergence of the TCF7L2–carvacrol complex compared to shorter simulation times. The protein backbone RMSD showed an initial relaxation phase and then stabilized after approximately 40 ns, fluctuating within ~ 0.25–0.35 nm, indicating preservation of the global structural fold. Importantly, the ligand RMSD remained consistently low (~ 0.01–0.02 nm) throughout the full 200 ns trajectory, confirming that carvacrol remained tightly retained in the binding cavity without dissociation or major reorientation. Similarly, the binding pocket RMSD stabilized after ~ 30–40 ns and remained confined around ~ 0.30–0.35 nm, supporting local convergence and structural stability of the active-site region during ligand accommodation. In agreement with these findings, the radius of gyration remained stable (17.3–18.2 Å), with the later stage predominantly maintained within ~ 17.4–17.7 Å, indicating that ligand binding did not induce unfolding or structural collapse. The SASA profile also remained stable across the trajectory (approximately ~ 970–1015 Å² after ~ 90 ns), while the hydrogen bond network remained persistent with stable fluctuations (~ 360–390 H-bonds), supporting a stable solvated environment and consistent polar interaction patterns. Finally, PCA analysis revealed clustering into dominant conformational basins during the later stage (~ 120–200 ns), providing additional evidence of convergence and equilibrated collective motions. Collectively, these results confirm that extending MD simulations to 200 ns resolves the convergence concern and supports the dynamic stability of the TCF7L2–carvacrol complex under near-physiological conditions.

As an example, diabetic mice (STZ) during carvacrol administration (20 mg/kg i.p) revealed after 4–6 weeks a most important decrease of fasting/random glucose, enhanced glucose tolerance, lowered triglycerides, and augmented hepatic enzyme activities (hexokinase, PFK, CS)[12]. On the same note, a combination of carvacrol (20 mg/kg oral) and rosiglitazone improved glucose-6-phosphatase and fructose-1,6-bisphosphatase activity and rescued glucokinase and G6PDH in HFD-induced type 2 diabetic mice[55]. In addition, carvacrol remarkably safeguarded the liver functions and ameliorated insulin resistance in db/db mice, lowering fasting glucose, lipids, ALT/AST, and regulating TLR4/NF κB and AKT/mTOR signaling pathways[56]. Mechanistic considerations also indicate that carvacrol can trigger PI3K/AKT/GLUT4 signaling and translocation of GLUT4, which we verified computationally via DFT calculations (HOMO-LUMO gap: 0.222 eV) and were able to identify binding interactions that may be responsible for these effects[14]. Lastly, carvacrol ameliorated glucose and lipid parameters in HFD/low-dose STZ rats through the regulation of short-chain fatty acids and the expression of GPR41/43 receptors[11]. Collectively, our computational results not only resonate with the metabolic enhancements and pathway activations observed by the experimental works but even offer structural insights on how carvacrol binds to a key genetic target in diabetes, TCF7L2.

The in-silico results presented here, based on the pharmacological evidence that can be found and translated into the biological sciences, give together strong reasons to think that carvacrol could be a potential therapeutic compound for diabetes mellitus. Analyses of ADMET parameters and ProTox 3.0 suggested favorable pharmacokinetics with high gastrointestinal absorption and blood-brain barrier permeability without violation of Lipinski's rule of five and suggesting drug-likeness and oral bioavailability. Moreover, carvacrol had a low predicted toxicity in the form of LD50 (810 mg kg-1), and did not cause hepatotoxicity, nephrotoxicity, or mutagenicity, supporting the pre-clinical safety margin. These pharmacological attributes are in line with previously-reported experimental data in which oral or intraperitoneal administration of carvacrol up to doses of 50 mg kg-1 did not result in adverse biochemical or histopathological effects in rodent models[13]. When compared to well-studied natural antidiabetic compounds, carvacrol shows computational efficacy and safety comparable to other compounds, if not more. Berberine, a clinically proven quinoline alkaloid extracted from the Berberis species, has been reported to increase glucose metabolism by activating the phosphorylation of the adenosine monophosphate-activated protein kinase (AMPK) and insulin receptor substrate 1/phosphatidyl inositol 3-kinase/Akt signaling pathway, which results in improved insulin sensitivity in type 2 diabetes models[57]. Likewise, Momordicosides isolated from *Momordica charantia* (bitter melon) display docking energies of the order of, and around − 9 to −12 kcal/mol against alpha floor amylase and DPP-IV in a way comparable with

their reported glucose-lowering and beta cell protective properties[58]. Coupled with its favourable ADMET and ProTox profile (high GI absorption and no mutagenicity or hepatotoxicity, LD50 = 810 mg/kg), these results highlight carvacrol as an extremely stable, low-toxicity and pharmacologically attractive scaffold for the future development of antidiabetic drugs.

Although the present study is based on in-silico modeling of the interaction of carvacrol with TCF7L2, these observations are supported by a growing body of experimental literature documenting antidiabetic and metabolic-regulatory effects of carvacrol in-vivo and in-vitro. For example, carvacrol administered at a dose of 25 and 50 mg/kg for 7 consecutive days in a streptozotocin (STZ)-induced diabetic rat model caused a significant suppression of hyperglycaemia and improvement in parameters linked to the development of diabetes[13]. Similarly, treatment of mice with 10–20 mg/kg carvacrol for six weeks before treatment with STZ or the high-fat diet improved glucose tolerance and reduced triglycerides, suggesting insulin sensitivity and hepatic carbohydrate-metabolizing enzyme activities[59]. In db/db mice, the mouse model of type 2 diabetes, carvacrol treatment reduced fasting glucose, improved dyslipidaemia, and improved biomarkers of hepatic and renal dysfunction[56]. Mechanistic studies also showed activation of PI3K/AKT signaling axis by carvacrol, which contributed to GLUT4 membrane translocation in diabetic mice with subsequent improvement in insulin sensitivity and uptake of glucose in target tissues[60]. In mediating models of diabetic vascular dysfunction, carvacrol decreased the inflammatory responses via the TLR4/NF-kB pathway and restored the endothelial integrity in db/db mice[61].

These experimental observations provide a biologically-based support for our in-silico results. In our analysis, carvacrol showed stable binding and dynamic stability within the active site of TCF7L2, suggesting a direct modulation of this key transcriptional regulator of β-cell function and insulin secretion. Since TCF7L2 regulates the Wnt/V-catenin pathway, insulin gene expression, and V-cell proliferation, the present data may link in-silico ligand-protein interactions with the phenotypic effects in the mouse, such as improved glucose tolerance and insulin sensitivity. Specifically, the in-vivo activation of PI3K/AKT/GLUT4 is consistent with the downstream effects of TCF7L2 modulation: dysregulation of TCF7L2 activity perturbs downstream insulin-signaling pathways and, consequently, alters GLUT4 translocation and glucose uptake in peripheral tissues. "Accordingly, our docking and molecular dynamics findings suggest that carvacrol may be able to exert antidiabetic effects not only through general antioxidant or anti-inflammatory mechanisms as described previously, but also directly via interaction with TCF7L2, thus modulating insulin-gene regulation at a molecular level. It should be noted that while the combination of in-silico and in-vivo evidence enhances the mechanistic plausibility for carvacrol as an antidiabetic agent, conclusive evidence requires experimental validation specifically for the ligand-TCF7L2 interaction. Such validation could include cellular assays for profiling TCF7L2 activity, transcriptional profiling of v-cell lines, or knockout/knockdown models. Nevertheless, the current study should be considered hypothesis-generating, and it advocates further wet-lab research instead of providing definitive proof of the efficacy of therapy.

This study provides robust evidence supporting the use of *Moringa oleifera* and its bioactive compounds, particularly Carvacrol, in developing antidiabetic therapies. The use of computational models has enabled us to efficiently identify potential drug candidates. Future in-vitro studies are necessary to further assess the reliability and efficacy of these compounds. Integrating novel computer model techniques in drug discovery could bridge the gap between medical experts and researchers, facilitating the development of effective treatments for diabetes mellitus[3].

Conclusion

The World Health Organization reported that diabetes mellitus is a multifactorial epidemic disorder in which multiple factors contribute to different complications. In the recent era, Carvacrol is well considered for its potential biological activities, such as antimicrobial, antioxidant, anticancer, and antidiabetic activities, that contribute to inhibiting certain enzymes that may reduce hyperglycemia in diabetic patients. Keeping in view the mortality and morbidity rate of diabetes is increasing among the global population, Carvacrol of *Moringa* essential oil constituents against diabetes mellitus was designed to check its potential effects on the health of human beings, which showed promising results in *in-silico* testing by ADMET profiling, pharmacophore, binding affinity, interactions, and remained stable with low RMSD values during molecular dynamic simulations.

Limitations future prospective

The prospects of this study involve advancing beyond in-silico analysis to validate the efficacy and safety of the developed drug against diabetes, utilizing phytochemicals extracted from *Moringa* and designed through computer-aided design. With *TCF7L2* identified as the receptor and carvacrol as the lead compound, the next steps entail comprehensive in-vitro and in-vivo analyses. This study represents the first in-silico screen for a new molecular target for carvacrol, providing a link between a well-known natural compound and a previously identified, yet uncharacterized, genetic regulator of type 2 diabetes. The mechanistic knowledge gained will lead to areas of investigation far outside of the traditional enzymatic target (alpha-amylase, dipeptidyl peptidase-IV (DPPIV)). It is recommended that future in-vitro studies should be focused on empirical validation of these findings, in particular, measurement of the effect of carvacrol on TCF7L2 transcriptional activity, β-cell function, and insulin secretion in available pancreatic cell lines (e.g., INS-1, MIN6) using luciferase reporter assays. Experimental confirmation of the predicted ligand-target interaction by functional modulation of glucose homeostasis would constitute an important point of connection between computational inference and experimental validation. These validations are crucial to ascertain the drug's therapeutic potential, safety profile, and mechanism of action in real biological systems. Additionally, further investigations could explore potential synergistic effects, dosage optimization, and long-term effects to fully assess the feasibility and viability of this

drug candidate. By bridging computational design with empirical experimentation, this research has the potential to contribute significantly to the development of novel therapeutic interventions for diabetes management.

Data availability

All data supporting the findings of this study, including PDB files, molecular structures, and associated computational parameter files, are available in a publicly accessible repository to ensure transparency and reproducibility. The complete dataset has been deposited in the Zenodo repository and can be accessed via the following link: [https://doi.org/10.5281/zenodo.15657382].

Received: 27 July 2025; Accepted: 17 February 2026
Published online: 20 February 2026

References

1. Bastaki, S. Diabetes mellitus and its treatment. *Dubai Diabetes Endocrinol. J.* **13**, 111–134 (2005).
2. Alam, U., Asghar, O., Azmi, S. & Malik, R. A. General aspects of diabetes mellitus. *Handb. Clin. Neurol.* **126**, 211–222 (2014).
3. Kaveeshwar, S. A. & Cornwall, J. The current state of diabetes mellitus in India. *Australas. Med. J.* **7**, 45 (2014).
4. Deshpande, A. D., Harris-Hayes, M. & Schootman, M. Epidemiology of diabetes and diabetes-related complications. *Phys. Ther.* **88**, 1254–1264 (2008).
5. Gloyn, A. L., Braun, M. & Rorsman, P. Type 2 diabetes susceptibility gene TCF7L2 and its role in β-Cell function. *Diabetes* **58**, 800 (2009).
6. Villareal, D. T. et al. TCF7L2 variant rs7903146 affects the risk of type 2 diabetes by modulating incretin action. *Diabetes* **59**, 479–485 (2010).
7. Lin, L. et al. ABCC8-related maturity-onset diabetes of the young (MODY12): A report of a Chinese family. *Front. Endocrinol.* **11**, 645 (2020).
8. Elbein, S. C. Role of calpain-10 gene variants in familial type 2 diabetes in Caucasians. *J. Clin. Endocrinol. Metab.* **87**, 650–654 (2002).
9. Saez, M. E. et al. The CAPN10 gene is associated with insulin resistance phenotypes in the Spanish population. *PLoS One* **3**, e2953 (2008).
10. Hattersley, A. T. Prime suspect: The TCF7L2 gene and type 2 diabetes risk. *J. Clin. Invest.* **117**, 2077–2079 (2007).
11. Sun, Y. et al. Carvacrol improves blood lipid and glucose in rats with type 2 diabetes mellitus by regulating short-chain fatty acids and the GPR41/43 pathway. *Korean J. Physiol. Pharmacol.* **28**, 1–10 (2024).
12. Li, Y. et al. Effect of long-term treatment of Carvacrol on glucose metabolism in Streptozotocin-induced diabetic mice. *BMC Complement. Med. Ther.* **20**, 1–8 (2020).
13. Bayramoglu, G. et al. Carvacrol partially reverses symptoms of diabetes in STZ-induced diabetic rats. *Cytotechnology* **66**, 251–257 (2014).
14. Hou, N. et al. Carvacrol attenuates diabetic cardiomyopathy by modulating the PI3K/AKT/GLUT4 pathway in diabetic mice. *Front. Pharmacol.* **10**, 998 (2019).
15. Kim, D. E., Chivian, D. & Baker, D. Protein structure prediction and analysis using the Robetta server. *Nucleic Acids Res.* **32**, W526–W531 (2004).
16. Laskowski, R., MacArthur, M. & Thornton, J. PROCHECK: validation of protein-structure coordinates. (2006).
17. Hasan, M. et al. Computational study and homology modeling of phenol hydroxylase: key enzyme for phenol degradation. *Int. J. Comput. Bioinfo Silico Model.* **4**, 691–698 (2015).
18. Benkert, P., Künzli, M. & Schwede, T. QMEAN server for protein model quality estimation. *Nucleic Acids Res.* **37**, W510–W514 (2009).
19. Szklarczyk, D. et al. STRING v10: protein–protein interaction networks, integrated over the tree of life. *Nucleic Acids Res.* **43**, D447–D452 (2015).
20. Naveed, M. et al. The natural breakthrough: Phytochemicals as potent therapeutic agents against spinocerebellar ataxia type 3. *Sci. Rep.* **14**, 1529 (2024).
21. Daina, A., Michielin, O. & Zoete, V. SwissADME: A free web tool to evaluate pharmacokinetics, drug-likeness and medicinal chemistry friendliness of small molecules. *Sci. Rep.* **7**, 42717 (2017).
22. Banerjee, P., Kemmler, E., Dunkel, M. & Preissner, R. ProTox 3.0: A webserver for the prediction of toxicity of chemicals. *Nucleic Acids Res.* https://doi.org/10.1093/nar/gkae303 (2024).
23. Jiménez, J., Doerr, S., Martínez-Rosell, G., Rose, A. S. & De Fabritiis, G. DeepSite: Protein-binding site predictor using 3D-convolutional neural networks. *Bioinformatics* **33**, 3036–3042 (2017).
24. Wadood, A. et al. In-silico drug design: An approach which revolutionarised the drug discovery process. *OA Drug Design and Delivery* **1**, 3 (2013).
25. Vilar, S., Cozza, G. & Moro, S. Medicinal chemistry and the molecular operating environment (MOE): Application of QSAR and molecular docking to drug discovery. *Curr. Top. Med. Chem.* **8**, 1555–1572 (2008).
26. Kashefolgheta, S., Wang, S., Acree, W. E. & Hünenberger, P. H. Evaluation of nine condensed-phase force fields of the GROMOS, CHARMM, OPLS, AMBER, and OpenFF families against experimental cross-solvation free energies. *Phys. Chem. Chem. Phys.* **23**, 13055–13074 (2021).
27. Zaheer, M., Ali, N., Javed, H., Munir, R. & Jamil, N. Uncovering the impact of SARS-CoV2 spike protein variants on human receptors: A molecular dynamics docking and simulation approach. *J. Infect. Public Health.* **16**, 1544–1555 (2023).
28. Nguyen, T. T., Viet, M. H. & Li, M. S. Effects of water models on binding affinity: Evidence from All-Atom simulation of binding of Tamiflu to A/H5N1 neuraminidase. *Sci. World J.* **2014**, 536084. https://doi.org/10.1155/2014/536084 (2014).
29. Leontyev, I. V. & Stuchebrukhov, A. A. Polarizable mean-field model of water for biological simulations with AMBER and CHARMM force fields. *J. Chem. Theory Comput.* **8**, 3207–3216. https://doi.org/10.1021/ct300011h (2012).
30. Rahman, S. U. et al. Innovative phytochemicals based in-silico drug design and molecular dynamics simulation targeting norovirus induced gastroenteritis. *J. Mol. Struct.* https://doi.org/10.1016/j.molstruc.2025.141733 (2025).
31. Inan, D., Karageçili, S., Ali, N. & Ali, A. AI-fragmented derivatives of methotrexate to design effective and safer DHFR inhibitor: A computational breakthrough for ectopic pregnancy therapy. *Comput. Biol. Chem.* **122**, 108906. https://doi.org/10.1016/j.compbiolchem.2026.108906 (2026).
32. Nagamalla, L. et al. Identification of novel AXL kinase inhibitors using ligand-based pharmacophore screening and molecular dynamics simulations. *Crystals* **12**, 1158 (2022).
33. Naveed, M. et al. Assessment of Melia azedarach plant extracts activity against hypothetical protein of mycobacterium tuberculosis via GC-MS analysis and in-silico approaches. *J. Comput. Biophys. Chem.* **1**, 22 (2023).
34. Pourbasheer, E., Bazl, R. & Amanlou, M. Molecular docking and 3D-QSAR studies on the MAPKAP-K2 inhibitors. *Med. Chem. Res.* **23**, 2252–2263 (2014).

35. la De Roche, M., Worm, J. & Bienz, M. The function of BCL9 in Wnt/β-catenin signaling and colorectal cancer cells. *BMC cancer* **8**, 1–13 (2008).
36. Stankiewicz, T. R., Gray, J. J., Winter, A. N. & Linseman, D. A. C-terminal binding proteins: Central players in development and disease. *Biomolecular concepts* **5**, 489–511 (2014).
37. Byun, J. S. & Gardner, K. C-terminal binding protein: A molecular link between metabolic imbalance and epigenetic regulation in breast cancer. *Int. J. Cell Biol.* **2013**, 647975 (2013).
38. Arise, R. O., Aburo, O. R., Farohunbi, S. T. & Adewale, A. A. Antidiabetic and antioxidant activities of ethanolic extract of dried flowers of *Moringa oleifera* in streptozotocin-induced diabetic rats. *Acta Fac. Med. Naiss.* **33**, 259 (2016).
39. Fatoumata, B., Mohamet, S., Sambou, J. K., MbackÃ, M. & El HadjiMakhtar, B. Antidiabetic properties of *Moringa oleifera*: A review of the literature. *J. Diabetes Endocrinol.* **11**, 18–29 (2020).
40. Chaachouay, N. & Zidane, L. Plant-derived natural products: A source for drug discovery and development. *Drugs Drug Candidates* **3**, 184–207 (2024).
41. Atanasov, A. G. et al. Discovery and resupply of pharmacologically active plant-derived natural products: A review. *Biotechnol. Adv.* **33**, 1582–1614 (2015).
42. Gupta, R. et al. Evaluation of antidiabetic and antioxidant activity of *Moringa oleifera* in experimental diabetes. *J. Diabetes* **4**, 164–171 (2012).
43. Miró, M. V. et al. Plant-derived compounds as a tool for the control of gastrointestinal nematodes: Modulation of abamectin pharmacological action by carvone. *Front. Vet. Sci.* **7**, 601750 (2020).
44. Barreto, G. E. & Sahebkar, A. *Pharmacological Properties of Plant-Derived Natural Products and Implications for Human Health* Vol. 1308 (Springer Nature, 2021).
45. Famuyiwa, S. O. et al. Comprehensive computational studies of naturally occurring Kuguacins as antidiabetic agents by targeting Visfatin. *Chem. Afr.* **6**, 1415–1427. https://doi.org/10.1007/s42250-023-00604-8 (2023).
46. Famuyiwa, S. O. et al. Investigating the multitargeted anti-diabetic potential of cucurbitane-type triterpenoid from *Momordica charantia*: An LC-MS, docking-based MM\GBSA and MD simulation study. *J. Biomol. Struct. Dyn.* **43**, 1159–1170. https://doi.org/10.1080/07391102.2023.2291174 (2025).
47. Al-Malki, A. L. & El Rabey, H. A. The antidiabetic effect of low doses of *Moringa oleifera* Lam. seeds on streptozotocin induced diabetes and diabetic nephropathy in male rats. *Biomed Res. Int.* https://doi.org/10.1155/2015/381040 (2015).
48. Villarruel-López, A. et al. Effect of Moringa oleifera consumption on diabetic rats. *BMC Complement. Altern. Med.* **18**, 1–10 (2018).
49. Aja, P., Igwenyi, I., Okechukwu, P., Orji, O. & Alum, E. Evaluation of anti-diabetic effect and liver function indices of ethanol extracts of *Moringa oleifera* and *Cajanus cajan* leaves in alloxan induced diabetic albino rats. *Glob. Veterinaria* **14**, 439–447 (2015).
50. Chivian, D. et al. Automated prediction of CASP-5 structures using the Robetta server. *Proteins Struct. Funct. Genet.* **53**, 524–533 (2003).
51. Saha, R. & Prasad, B. V. In silico approach for designing of a multi-epitope based vaccine against novel Coronavirus (SARS-COV-2). *BioRxiv* 2020.2003. 2031.017459 (2020).
52. Astria, M. V. et al. In silico analysis of 14-deoxy 11, 12-didehydro andrographolide (AGP 2) from Sambiloto (*Andrographis paniculata*) as drug candidate against SARS-CoV-2. *HAYATI J. Biosci.* **30**, 480–490 (2023).
53. Fareed, M. M. et al. In silico drug screening analysis against the overexpression of PGAM1 gene in different cancer treatments. *BioMed Research International* 1–7 (2021). (2021).
54. Dias, R., de Azevedo, J. & Walter, F. Molecular docking algorithms. *Curr. Drug Targets* **9**, 1040–1047 (2008).
55. Ezhumalai, M., Radhiga, T. & Pugalendi, K. V. Antihyperglycemic effect of carvacrol in combination with rosiglitazone in high-fat diet-induced type 2 diabetic C57BL/6J mice. *Mol. Cell. Biochem.* **385**, 23–31 (2014).
56. Zhao, W. et al. Protective effect of carvacrol on liver injury in type 2 diabetic db/db mice. *Mol. Med. Rep.* **24**, 741 (2021).
57. Utami, A. R., Maksum, I. P. & Deawati, Y. Berberine and its study as an antidiabetic compound. *Biol. (Basel)* https://doi.org/10.3390/biology12070973 (2023).
58. Xu, B. et al. Bioactives of *Momordica charantia* as potential anti-diabetic/hypoglycemic agents. *Molecules* **27**, 2175 (2022).
59. Li, Y. et al. Effect of long-term treatment of carvacrol on glucose metabolism in Streptozotocin-induced diabetic mice. *BMC Complement. Med. Ther.* **20**, 142. https://doi.org/10.1186/s12906-020-02937-0 (2020).
60. Hou, N. et al. Carvacrol attenuates diabetic cardiomyopathy by modulating the PI3K/AKT/GLUT4 pathway in diabetic mice. *Front. Pharmacol.* https://doi.org/10.3389/fphar.2019.00998 (2019).
61. Zhao, W., Deng, C., Han, Q., Xu, H. & Chen, Y. Carvacrol may alleviate vascular inflammation in diabetic db/db mice. *Int. J. Mol. Med.* **46**, 977–988 (2020).

Acknowledgements
The authors would like to sincerely thank Dr. Muhammad Naveed and Dr. Hira Mubeen for their valuable guidance, encouragement, and motivation throughout the course of this study.

Author contributions
Amna Saleem, Nouman Ali, and Adeeba Ali conceived the study, performed the analyses, and wrote the initial draft of the manuscript. Nouman Ali supervised the research and provided critical input throughout manuscript preparation. Shakhlokhon Kurbanova contributed to the revision of methodology and addressing reviewer comments. Erkabay Eshchanov assisted with refining the results and discussion during revision. All authors reviewed, edited, and approved the final version of the manuscript.

Declarations

Competing interests
The authors declare no competing interests.

Ethics statement
This study did not involve any human participants, animal experiments, or data from social media platforms; therefore, ethical approval and informed consent were not required. All computational analyses, including molecular docking, ADMET prediction, DFT calculations, and molecular dynamics simulations, were conducted using publicly available databases and software tools in accordance with institutional and international ethical standards for in-silico research.

Additional information

Correspondence and requests for materials should be addressed to A.S. or N.A.